iScience

CellPress
OPEN ACCESS

Article

Identifying States of Collateral Sensitivity during the Evolution of Therapeutic Resistance in Ewing's Sarcoma

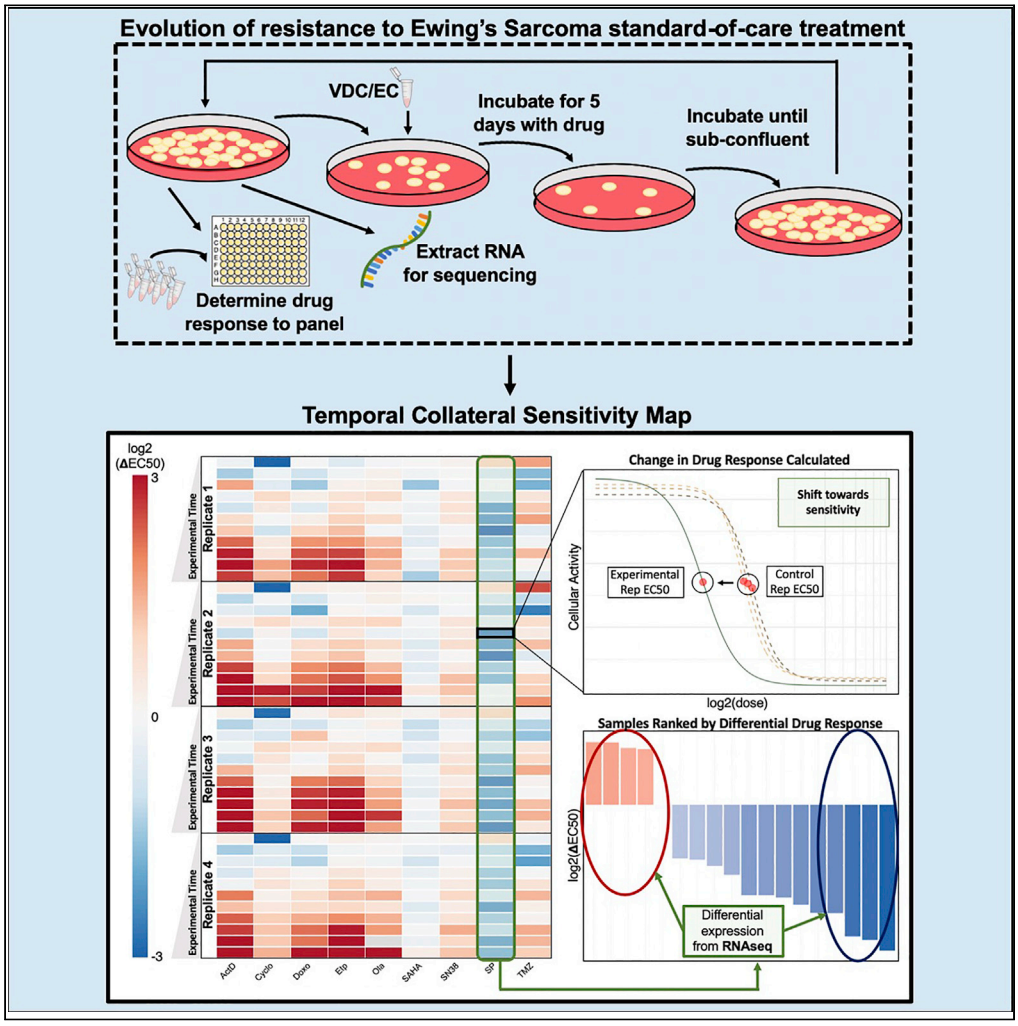

Jessica A. Scarborough, Erin McClure, Peter Anderson, ..., Stephen L. Lessnick, Masahiro Hitomi, Jacob G. Scott

scottj10@ccf.org

HIGHLIGHTS

Ewing's sarcoma cell lines were evolved to become resistant to standard chemotherapy

A temporal collateral sensitivity map shows response to alternative drugs over time

Collateral drug response is repeatable in some instances and stochastic in others

Differential gene expression elucidates potential biomarkers of drug response

Scarborough et al., iScience *23*, 101293
July 24, 2020
https://doi.org/10.1016/j.isci.2020.101293

iScience

CellPress
OPEN ACCESS

Article

Identifying States of Collateral Sensitivity during the Evolution of Therapeutic Resistance in Ewing's Sarcoma

Jessica A. Scarborough,[1,2] Erin McClure,[1,3] Peter Anderson,[4] Andrew Dhawan,[5] Arda Durmaz,[1,2] Stephen L. Lessnick,[6,7] Masahiro Hitomi,[1] and Jacob G. Scott[1,2,8,9,*]

SUMMARY

Advances in the treatment of Ewing's sarcoma (EWS) are desperately needed, particularly in the case of metastatic disease. A deeper understanding of collateral sensitivity, where the evolution of therapeutic resistance to one drug aligns with sensitivity to another drug, may improve our ability to effectively target this disease. For the first time in a solid tumor, we produced a temporal collateral sensitivity map that demonstrates the evolution of collateral sensitivity and resistance in EWS. We found that the evolution of collateral resistance was predictable with some drugs but had significant variation in response to other drugs. Using this map of temporal collateral sensitivity in EWS, we can see that the path toward collateral sensitivity is not always repeatable, nor is there always a clear trajectory toward resistance or sensitivity. Identifying transcriptomic changes that accompany these states of transient collateral sensitivity could improve treatment planning for patients with EWS.

INTRODUCTION

Ewing's sarcoma (EWS) is the second most common primary malignant bone cancer in children (Ries, 1999; Esiashvili et al., 2008). Localized disease has a 50%–70% 5-year survival rate, and metastatic disease has a devastating 18%–30% 5-year survival rate (Esiashvili et al., 2008; Grier et al., 2003; Hunold et al., 2006). Advances in the treatment of EWS are desperately needed, particularly in the case of metastatic disease. Unfortunately, all recent attempts to improve the chemotherapy regimen for EWS have only yielded modest results for non-metastatic cancer with little to no impact on the course of metastatic disease (Grier et al., 2003; Huang and Lucas, 2010). Researchers have tried adding ifosfamide and etoposide to standard EWS chemotherapy, increasing the drug doses administered, and decreasing the interval between doses, all without meaningful improvement to metastatic disease outcomes (Grier et al., 2003; Huang and Lucas, 2010; Womer et al., 2012). Even when treatment is initially successful, EWS often evolves therapeutic resistance, which ultimately leads to disease relapse (Ahmed et al., 2014). A deeper understanding of the evolutionary dynamics at play as EWS develops therapeutic resistance may improve our ability to effectively target this disease (Scott and Marusyk, 2017).

During the evolution of therapeutic resistance, both bacteria and cancer can exhibit a phenomenon termed collateral sensitivity, where resistance to one drug aligns with sensitivity to another drug (Pluchino et al., 2012; Pál et al., 2015; Hall et al., 2009). Likewise, collateral resistance occurs when resistance to one drug aligns with resistance to another drug. The relationship between genotype (e.g., gene expression, somatic mutations) and fitness of a cell line can be represented by a fitness landscape. In the case of drug response, we define fitness as the EC50 of a cell line to a given drug, where increasing EC50 denotes higher fitness in the presence of this drug. EC50 is defined as the concentration of drug that achieves half-maximal effective response. Of importance, a cell line with the same genotype may have varying fitnesses (EC50s) under the selection pressure of different drugs.

In collateral resistance, the fitness landscapes of the organism (bacteria or cancer) in the presence of each drug would show "positive correlation" (Nichol et al., 2019). This is because genotypic changes that cause increased fitness in the presence of the first drug also allow increased fitness in the presence of the second drug as well. Next, comparing fitness landscapes in the setting of collateral sensitivity will show "negative

[1]Translational Hematology and Oncology Research, Taussig Cancer Institute, Cleveland Clinic, Cleveland, OH 44106, USA

[2]Systems Biology and Bioinformatics Department, School of Medicine, Case Western Reserve University, Cleveland OH 44106, USA

[3]Morsani College of Medicine, University of South Florida, Tampa, FL 33612, USA

[4]Heme/Onc/BMT, Cleveland Clinic, Cleveland, OH 44106, USA

[5]Neurological Institute, Cleveland Clinic, Cleveland, OH 44106, USA

[6]Center for Childhood Cancer and Blood Diseases, Abigail Wexner Research Institute at Nationwide Children's Hospital, Columbus, OH 43205, USA

[7]Division of Pediatric Heme/Onc/BMT, The Ohio State University, Columbus, OH 43205, USA

[8]Department of Radiation Oncology, Cleveland Clinic, Cleveland, OH 44106, USA

[9]Lead Contact

*Correspondence: scottj10@ccf.org

https://doi.org/10.1016/j.isci.2020.101293

Drug Name	Abbreviation	Class
Dactinomycin	ActD	Antineoplastic antibiotic
Cyclophosphamide	Cyclo	Alkylating agent
Ifosfamide	Ifo	Alkylating agent
Doxorubicin	Doxo	Anthracycline
Etoposide	Etp	Topoisomerase II inhibitor
Olaparib	Ola	PARP inhibitor
Pazopanib	Paz	Tyrosine kinase inhibitor
Vorinostat	SAHA	Histone deacetylase inhibitor
Irinotecan (active metabolite)	SN38	Topoisomerase I inhibitor
SP-2509	SP	[l] Lysine-specific demethylase 1 inhibitor
Temozolomide	TMZ	Alkylating agent
Vincristine	Vin	Alkaloid
Sodium thiosulfate	NaThio	Drug activation reagent

Table 1. All Drugs Referenced in the Study, Their Abbreviations, and Classifications

correlation," where genotypic changes leading to increased fitness in the presence of the first drug will cause decreased fitness in the presence of the second drug. Finally, comparing fitness landscapes in the presence of different treatments will not always demonstrate clear positive or negative correlation. Instead, the evolution of resistance to one drug may lead to variable changes in response to the second drug. In this setting, the evolutionary landscapes would be "uncorrelated." Here, predictive models would be especially useful in treatment planning, as relative collateral sensitivity or resistance cannot be inferred based solely on treatment history.

In the case of collateral sensitivity, a clinician could ideally control disease progression by switching to a collaterally sensitive drug whenever resistance develops. Even if the illness was never completely eradicated, the pathogen or neoplasm would be dampened enough to minimize harm to the patient. Yet evolution is rarely so easy to predict. Several studies have aimed to identify examples of collateral sensitivity in either bacteria or cancer, and many have shown that exposure to identical therapies has resulted in different responses between evolutionary replicates (Imamovic and Sommer, 2013; Munck et al., 2014; Nichol et al., 2015, 2019; Zhao et al., 2016; Dhawan et al., 2017; Maltas and Wood, 2019). Additionally, Zhao et al. examined changes in collateral sensitivity in acute lymphoblastic leukemia (ALL) over time (Zhao et al., 2016). Here, they produced temporal collateral sensitivity maps to show how drug response evolved over time and between evolutionary replicates (Zhao et al., 2016). Although Zhao et al. did examine these changes through time, many collateral sensitivity experiments compare only initial and final drug responses after resistance to the primary treatment has evolved (Dhawan et al., 2017; Nichol et al., 2019). These intermediate steps are crucial for determining whether the evolution of therapeutic resistance leads to a collateral fitness landscape that is consistently positively/negatively correlated or uncorrelated through time.

For the first time in a solid tumor, we examine the repeatability of collateral sensitivity across time as cells evolve resistance to standard treatment. In doing so, we use two EWS cell lines, A673 and TTC466. The A673 cell line contains the *t(11;22)* translocation resulting in the *EWSR1/FLI1* gene fusion (Szuhai et al., 2006; Martınez-Ramırez et al., 2003). This fusion is the most common genetic aberration found in 90%–95% EWS tumors (Sankar et al., 2014; Szuhai et al., 2006). In contrast, the TTC466 cell line has a *t(21;22)* translocation resulting in the EWS-ERG gene fusion, which occurs only in 5%–10% of EWS tumors (Sankar et al., 2014; Szuhai et al., 2006). After splitting the cell lines into evolutionary replicates, they were exposed to standard chemotherapy and their response to a panel of drugs was assessed over time. All drugs included in this study may be found in Table 1. We hypothesize that Ewing's sarcoma cell lines repeatedly

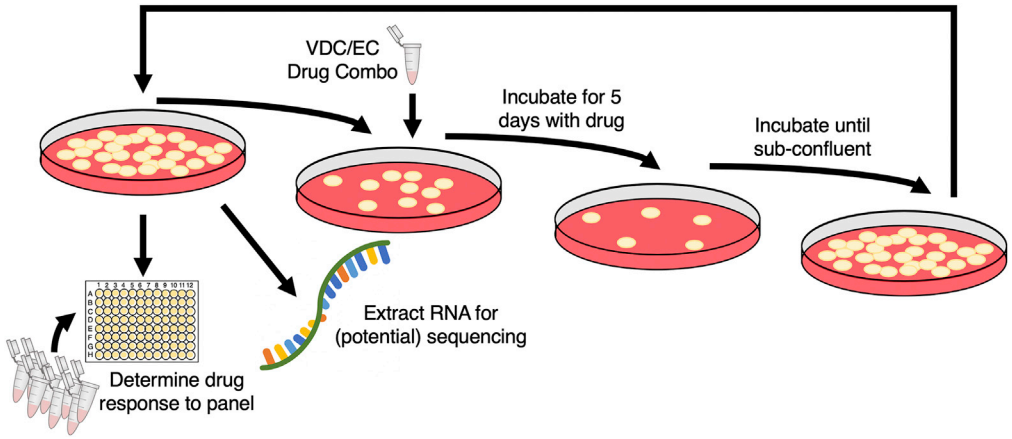

Figure 1. Overview of Experimental Evolution of Resistance in Ewing's Sarcoma Cell Lines

As cells recovered from each exposure, cells were tested for their sensitivity to a panel of drugs and samples were frozen for potential use in RNA sequencing. The drug dosage was only increased once throughout the experiment, at the fifth exposure to the VDC combination, described in Transparent Methods. Although each cell line began with five experimental and three control evolutionary replicates, the A673 cell line lost one experimental replicate owing to contamination.

exposed to standard chemotherapy will demonstrate divergent evolutionary paths between evolutionary replicates despite nearly identical experimental conditions and initial genotype. Finding patterns of collateral resistance (positively correlated landscapes), sensitivity (negatively correlated landscapes), or variation (uncorrelated landscapes) within these divergent paths may provide useful insight in exploring new treatment options for patients with EWS.

RESULTS

The Long-Term Evolution of Therapeutic Resistance

This work examines the evolution of collateral sensitivity and resistance in two EWS cell lines during repeated exposure to a standard chemotherapy regimen over time. At the onset of the experiment, each cell line was split into eight evolutionary replicates, five experimental and three control. Owing to contamination, Replicate 2 from the A673 cell line was excluded from the analysis, leaving four experimental and three control replicates in this cell line. Each experimental evolutionary replicate then underwent the same drug cycling, as demonstrated in Figure 1. Briefly, experimental replicates were incubated in cycles of vincristine-doxorubicin-cyclophosphamide (VDC) and etoposide-cyclophosphamide (EC) combinations (Grier et al., 2003). This procedure models standard of care given to patients with EWS, which consists of cycles of VDC and etoposide-ifosfamide (EI) combinations. Because ifosfamide requires metabolic activation and no activated compound is commercially available, we chose to substitute ifosfamide with cyclophosphamide, as these compounds are analogs (Fleming, 1997). Control replicates were maintained in only vehicle control. More details can be found in Transparent Methods.

After proliferating to sub-confluent density in maintenance medium, a fraction of cells from all evolutionary replicates were snap frozen for RNA extraction, another fraction underwent drug sensitivity assays to 12 drugs, and another fraction of the cells were plated for exposure to the next cycle of the alternate drug combination. For each drug at each time point, the EC50 of each evolutionary replicate was derived by fitting the drug-response triplicate data to a four-parameter log-logistic model as described in Transparent Methods. A plot of all dose-response triplicates with their estimated EC50 can be found in the GitHub Repository referred to in Data and Code Availability.

Discerning Changes in Chemo-Sensitivity and -Resistance across Time

Figures 2 and 3 display the changes in drug response to nine agents over time in the A673 cell line. In addition to the nine drugs displayed in this figure, two additional drugs (Pazopanib and Vincristine) and a drug

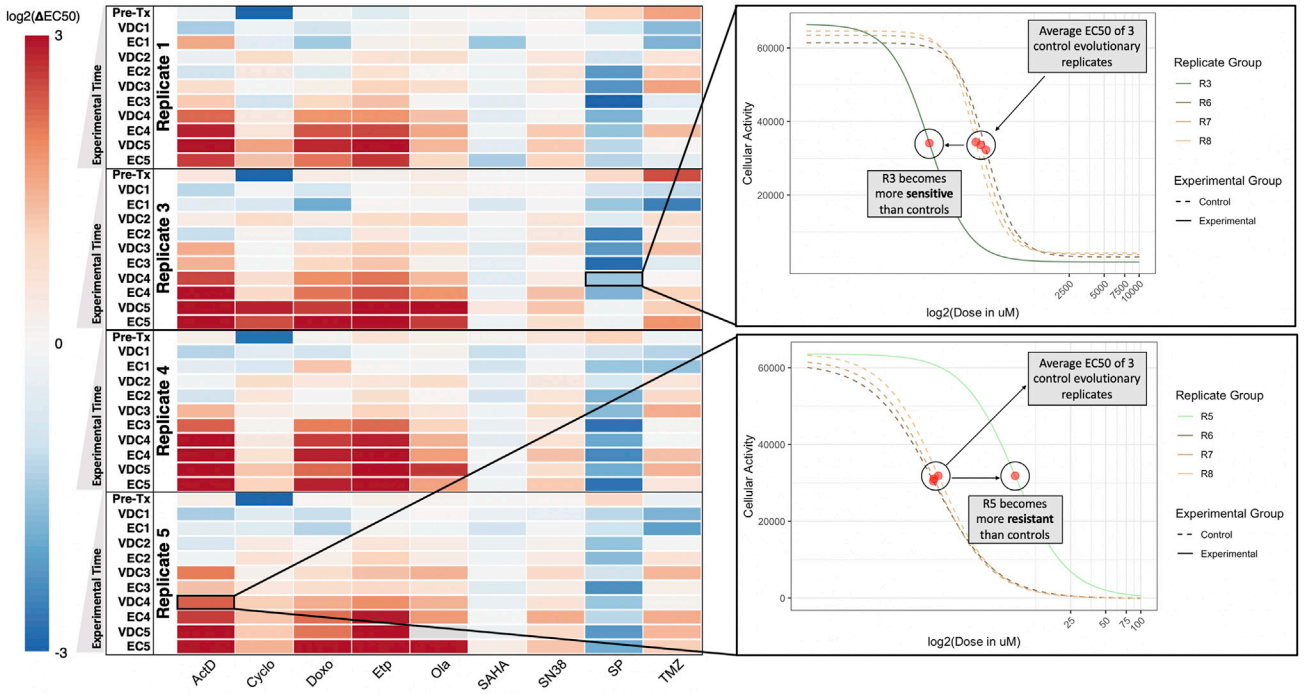

Figure 2. Temporal Collateral Sensitivity Map Representing EC50 Changes to a Panel of Drugs as the A673 Cell Line Develops Resistance to Standard Treatment

Left: A heatmap representing how the EC50 to a panel of nine drugs changes in four A673 cell line evolutionary replicates as they are exposed to the VDC/EC drug combinations over time. Color represents the $\log_2$ fold change of EC50 to a drug (columns) for a replicate at a given evolutionary time point (rows) compared with the average EC50 of the three control evolutionary replicates at the corresponding time point. Values above $\log_2(3)$ or below $\log_2(-3)$ are represented by $\log_2(3)$ and $\log_2(-3)$, respectively. Time points are denoted as the drug combination that a given replicate has recently recovered from. For example, the data representing dose-response models after the first application of the VDC drug combination would be labeled with VDC1. Of note, the EC50 of olaparib in Replicate 5 at the VDC5 time point is indeterminate owing to a poorly fit dose-response model. This value in the heatmap is denoted as gray, but Figure S1 remains uncensored. **Right:** Top, a plot of the dose-response curves for Replicate 3 and all control replicates (Replicates 6, 7, 8) in response to SP-2509 (SP) at the VDC4 time point. Bottom, a plot of the dose-response curve for Replicate 5 and all control replicates in response to dactinomycin at the VDC4 time point. Cellular activity is measured by enzymatic conversion of alamarBlue, normalized to background florescence. Estimated EC50 for each replicate is denoted with a red circle. These two dose-response plots demonstrate how the heatmap (left) values were calculated, where the control EC50 values are averaged, and the heatmap values represent the $\log_2$ fold change between a given replicate and this mean EC50 value.

activation reagent (sodium thiosulfate) were included in the drug sensitivity assays. Data for these drugs are included in Figures S1 and S2.

Unlike the A673 cell line, the TTC466 cell line develops resistance to only a few of the tested drugs, and when it is developed, it is not maintained across evolutionary time. It is unsurprising, therefore, to see that Figures S3 and S4 demonstrate that changes in collateral sensitivity responses are not significantly different between experimental and control replicates for the TTC466 cell line. As such, we focus our analysis on the A673 cell line, and the heatmap and point-range plots for the TTC466 cell line can be found in Figures S3 and S4, respectively.

Figure 2 shows a temporal collateral sensitivity map that represents the $\log_2$ fold change of EC50 to a drug (columns) for an experimental replicate at a given time point (rows) compared with the average EC50 of the three control evolutionary replicates to the same drug, at that time point. In the top right of the figure, we see the drug response of Replicate 3 to SP-2509 after its fourth exposure to VDC (VDC4), along with the three control evolutionary replicates at this time point. This example demonstrates a move toward sensitivity in the experimental replicate. In the bottom right, we can interrogate Replicate 5 at the same time point in response to dactinomycin, where the EC50 of this experimental replicate is more resistant than the control replicates. The temporal collateral sensitivity maps found in Figures S1 and S3 include the $\log_2$ fold change for each control evolutionary replicate from the average of the three control evolutionary

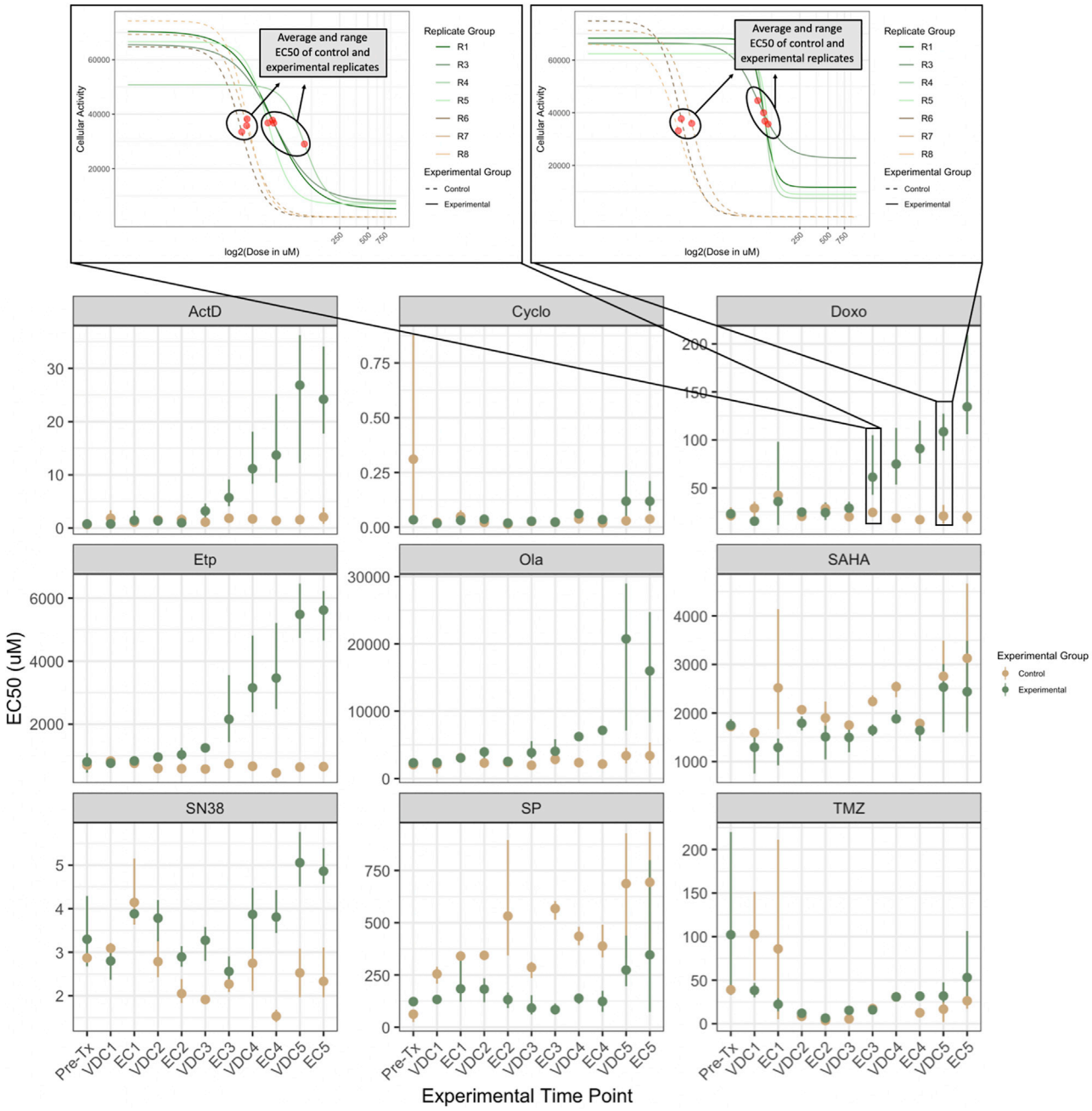

Figure 3. Point-Range Plots Demonstrating EC50 Changes in A673 Experimental and Control Replicates Over Time

Bottom: Point-range plots representing the changes in drug response to a panel of nine drugs. Experimental time points (x axis) represent which step in the drug cycle the replicates have just recovered from. Points on the plot represent the average EC50 for the group, either experimental or control. Lines represent the range for the entire group. The EC50 of olaparib for Replicate 5 after the fifth exposure to VDC is indeterminate owing to a poorly fit dose-response model and has been removed from this drug's VDC5 time point experimental group EC50 average and range calculations. This value has not been censored in Figures S1 and S2. The y axis of all the point-range plots has μM units, except Cyclo, where the unit is percent of chemically activated 4-hydroxycyclophosphamide solution by volume. **Top:** Two plots demonstrating a more detailed view of the dose-response data represented at the EC3 and VDC5 time points in the Doxo point-range chart. Cellular activity is measured by enzymatic conversion of alamarBlue, normalized to background florescence. Comparing these two plots shows the clear divergence in drug response between experimental and control evolutionary replicates as the treatment regimen continued.

replicates at the corresponding time point. Ideally, this value will be close to zero (white), because the three control replicates should have similar EC50s.

Figure 3 contains point-range plots for the nine drugs included in our analysis demonstrating the average and range of EC50 values for experimental and control replicates at each time point in the experiment. In response to doxorubicin, the control replicates remained stable across each progressive time point, but the experimental replicates became increasingly more resistant as they were repeatedly exposed to standard treatment. Examining these point-range plots also allows us to observe the overall stability of drug response in control replicates, which are not being evolved under the selection pressure of the VDC/EC drug cycling. For example, the EC50 range for control replicates to dactinomycin is so minimal that the lines representing range are not visible for most time points in the ActD panel of Figure 3. On the other hand, control replicates show significant variation in their response to SN38 and temozolomide (TMZ) at many time points.

The point-range plots in Figure 3 also allow for a more nuanced interrogation of the log-ratio changes displayed in Figure 2. For example, although all experimental replicates appear to become more sensitive in response to SP in Figure 2, the point-range plots in Figure 2 demonstrate that the control evolutionary replicates are becoming more resistant over time, whereas the experimental evolutionary replicates remain somewhat stable. This relative sensitivity between experimental and control evolutionary replicates is visualized as a negative $\log_2$ fold change in Figure 2. Yet, because the control, not experimental, evolutionary replicates changed over time, it is less clear whether or not this negative log-ratio should be interpreted as a move toward sensitivity in the experimental replicates. Early in the treatment series, the experimental and control replicates have very similar average EC50 measurements, demonstrating divergence over time. It is likely that the control conditions caused increased resistance to SP in the cell lines (leading to increasing EC50 in control replicates), whereas the application of the VDC/EC drug cycling regimen promoted sensitivity (leading to the appearance of stable EC50 through time).

Surveying the Stochasticity of Evolution

While examining Figures 2 and 3, we see predictable development of collateral resistance to some drugs, but evolutionary stochasticity and divergence in collateral response between replicates was observed in the response to others. For example, the cells were initially sensitive to dactinomycin and moved into a distinct state of collateral resistance in all replicates. This leads us to the preliminary conclusion that the evolutionary landscape of the cells under the VDC/EC selection pressure and the landscape of the cells under the dactinomycin selection pressure would show strong positive correlation. Next, all replicates acquired relatively consistent resistance to doxorubicin and etoposide over time, which is to be expected, because these two reagents are included in the treatment regimen. All replicates relatively consistently evolved from sensitive to resistant in response to olaparib, SN38, and temozolomide. In response to vorinostat (SAHA), all replicates appear to show minor sensitivity across time but no discernible trend toward greater sensitivity or resistance. Finally, there was moderate sensitivity to SP seen in all A673 replicates, again with no discernible trends through time. Owing to the variation in response to SAHA or SP over time, we would conclude that the fitness landscapes of cells exposed to these drugs compared with the landscapes of cells exposed to VDC/EC are relatively uncorrelated.

Unexpectedly, most replicates acquired only mild resistance to cyclophosphamide, a drug that is included in both cycles of the treatment regimen. Additionally, one of the control evolutionary replicates has an outlier EC50 estimate, which causes the pre-treatment (Pre-Tx) experimental evolutionary replicates to appear more sensitive to cyclophosphamide than the control evolutionary replicates. Although this outlier replicate is likely experimental noise, as it does not remain an outlier at future time points, the dose-response model is well fit to the data and we determined that censoring this replicate's time point EC50 estimate would be inappropriate.

Differential Gene Expression Analysis Provides Insight into the Mechanisms of Drug Response

Eighteen samples from the A673 cell line were RNA sequenced, visualized in the left panel of Figure 4. All the samples were ranked based on their response to the 12 drugs included in the drug sensitivity panels. These rankings are visually represented in waterfall plots of the $\log_2$ fold change in EC50 for all sequenced samples against all drugs and can be seen in Figures S5–S16. For each drug, differential gene expression (DE) analysis was performed between samples that rank in the top and bottom third of responses toward

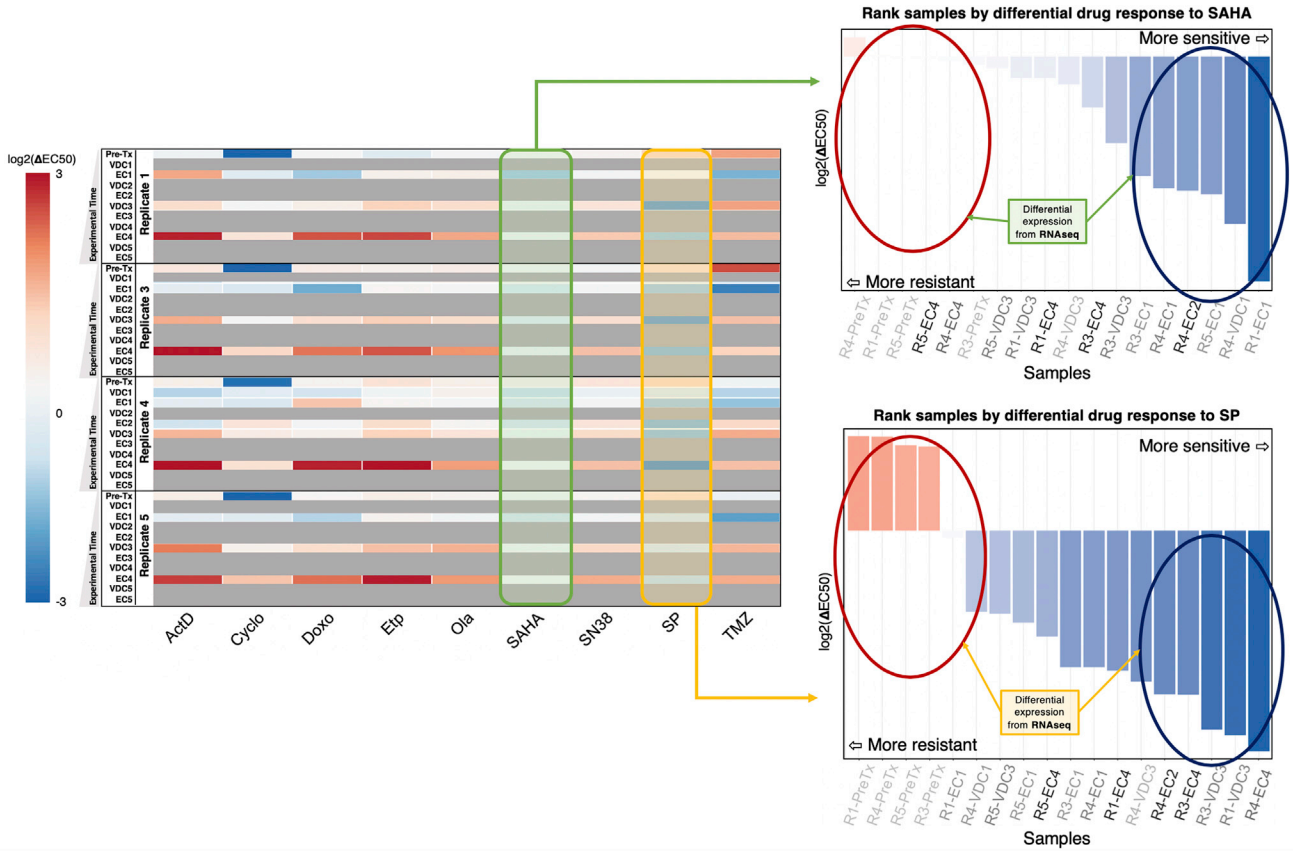

Figure 4. RNA Sequencing and Differential Gene Expression Analysis Provide Insight into States of Collateral Sensitivity and Resistance

Left: The temporal collateral sensitivity map from Figure 2, where all samples that were not sequenced are overlayed with gray. **Right:** Two waterfall plots representing the samples ranked by their responses to the two drugs, vorinostat (SAHA, top) and SP-2509 (SP, bottom). Sample labels on the x axis are represented by darker colors the longer they have been evolved in the evolutionary experiment.

the drug. Results for each drug's DE analyses, including the analyses highlighted below, may be found in Table S1.

In many cases, it is clear that ranking samples by their change in drug response also ranks them based on how long they have been exposed to the treatment regimen. Although this is not unexpected, interpreting the DE results in this context becomes more difficult. Significant differences in gene expression may be related to a sample's chemosensitivity/chemoresistance, but causation cannot be inferred, because these differentially expressed genes may simply be altered in response to continued exposure to the treatment regimen. We chose to highlight the DE analyses where ranking samples in response to a given drug did not consistently arrange them in the order that they were isolated from the drug-cycling treatment. To that end, the waterfall plots in Figures S5–S16 have darker sample labels (x axis) depending on how long they have been exposed to the treatment regimen (e.g., a sample label from the IE2 time point will be lighter than a sample from the IE3 time point). This makes it easier to visualize whether the time points are well distributed in the $\log_2$ fold change rankings.

The right panel of Figure 4 demonstrates how samples were ranked based on their response to vorinostat (SAHA) and SP-2509 (SP). Genes with significantly increased expression in a SAHA-resistant or SAHA-sensitive state are listed in Table 2, whereas genes with significantly increased expression in an SP-resistant or SP-sensitive state are listed in Table 3.

DISCUSSION

In this work, we evolved two EWS cell lines, A673 and TTC466, with repeated exposure to standard-of-care chemotherapy in order to investigate the evolution of collateral sensitivity and resistance through time. We

produced a temporal collateral sensitivity map to examine the drug sensitivity assays for nine of these drugs through time in the A673 cell line (see Figure 2). Likewise, Figure 3 demonstrates how the average and range EC50 between A673 experimental replicates and control replicates diverged as the experimental replicates continued the drug cycling treatment regimen. Figures S1 and S2 contain the drug response changes to all 12 drugs, with no censored data. Figures S3 and S4 also exhibit the changes in drug response within the TTC466 cell line; however, the main text focuses on the A673 cell line due to minimal shifts in resistance observed in response to the treatment regimen in the TTC466 cell line.

Figure 2 shows that, as the A673 experimental replicates were repeatedly exposed to the treatment regimen, states of collateral resistance emerge consistently toward some drugs, whereas responses to other agents remain variable. For example, despite no exposure to the drug, all replicates consistently moved to a state of collateral resistance toward dactinomycin, providing an example of positively correlated evolutionary landscapes. On the other hand, all replicates demonstrate possible collateral sensitivity to SP over time, although these results are not conclusive as the control evolutionary replicates moved toward resistance more than the experimental evolutionary replicates moved toward sensitivity. All replicates show variable minimal collateral sensitivity to SAHA, but no state of collateral resistance or sensitivity dominates for many time points or between replicates. Both of these drugs would have uncorrelated evolutionary landscapes in comparison with the landscape under the VDC/EC selection pressure. Additionally, these results imply that, although there are consistent changes that allow for collateral resistance to dactinomycin, these changes do not invariably cause a consistent pattern of collateral sensitivity to SAHA or SP. When collateral sensitivity or resistance cannot be consistently identified, gene signatures or other predictive models would be especially helpful in treatment planning.

We also note that the A673 experimental replicates consistently become more resistant to doxorubicin and etoposide, and there is a moderate shift toward resistance to cyclophosphamide. All of these drugs, in addition to vincristine, are included in the drug combination treatment regimen, which makes the evolution of resistance unsurprising. Although response to the drug combinations (VDC and EC) themselves was not measured, increased resistance to the treatment regimen was demonstrated by the decreased time required to reach sub-confluence after each cycle as time. As seen in Methods, this necessitated an increase in the final VDC drug combination concentration. Importantly, drug sensitivity changes in response to drug combinations may be the result of a variety of changes in response to the individual drug combination components, and this analysis would have been improved by measuring response to the drug combination triplicates and duplicates through time.

After analyzing the repeatability (or lack thereof) of the evolution of collateral sensitivity and resistance in the A673 EWS cell line, 18 samples from across various time points were sent for RNA sequencing (Figure 4). We identified significantly increased expression of ABCB1 (also known as MDR1) in the state of SAHA-resistance, seen in Table 2. This gene has previously been implicated in chemotherapeutic multi-drug resistance (Chen and Sikic, 2012). Additionally, CCL2 was found to have increased expression in a SAHA-sensitive state. Using an *in vitro* experiment, Gatti and Sevko et al. describe how adding SAHA to the temozolomide treatment of melanoma may stymie cancer growth by interfering with CCL2 signaling. This is consistent with increased CCL2 expression leading to SAHA sensitivity, as cells that are more reliant on CCL2 signaling could experience a stronger effect from its disruption (Gatti et al., 2014).

Next, we see a greater number of differentially expressed genes when examining response to SP than SAHA. SP inhibits lysine-specific demethylase 1 (LSD1, also known as KDMA1), which primarily acts as a histone demethylase (O'Leary et al., 2016). Increased expression of LSD1 has been implicated in many types of cancers (e.g., breast, prostate), and its targeted inhibition is being investigated for therapeutic potential in EWS (Yang et al., 2018). Owing to the novelty of LSD1 inhibitors (including SP-2509), there is very little known regarding genomic biomarkers of sensitivity or resistance. In Table 3, however, we see some notable trends in the significantly differentially expressed genes between good and poor responders to SP. First, many zinc protein fingers, which often play a role in transcriptional regulation, have increased expression in both SP-sensitive and -resistant states (Klug, 1999). Additionally, three TATA-box-binding-protein (TBP) associated factor (TAF) proteins have increased expression in SP-resistant states. Again, these genes are implicated in transcriptional regulation (Hampsey and Reinberg, 1997). Although these results do not imply any one mechanism for SP-sensitivity or -resistance, it is evident that the regulation of gene expression may play a significant role in the response to this drug.

Genes with ↑ Expression in SAHA-Sensitive State			
ACOT	ACPP	AHR	B3GNT5
CCL2	FOS	GAL	NUP188
RN7SL5P	SCNN1G	TRAV5	
Genes with ↑ Expression in SAHA-Resistant State			
ABCB1	KAZALD1	RPS26	SMAD6
TRGC1			

Table 2. Genes with Significant Differential Expression between SAHA-Resistant and SAHA-Sensitive Samples
Differential gene expression analysis was performed using EBSeq in R, with maxround set to 15 and FDR of 0.05.

As noted previously, states of collateral sensitivity and resistance are often not immutable. Instead, these states are frequently the result of many fleeting evolutionary contingencies. For instance, Nichol et al. demonstrated that, after *E. coli* evolved resistance to cefotaxime (a β-lactam antibiotic) in 60 evolutionary replicates, there were highly heterogeneous changes in collateral sensitivity and resistance to alternative antibiotics (Nichol et al., 2019). Genotypic heterogeneity was discovered as well, with five variants of the β-lactamase gene, which likely played a role in the variable drug responses. Additionally, Dhawan et al. derived cell lines of ALK-positive non-small cell lung cancer, where each cell line was resistant to a second-line therapy (Dhawan et al., 2017). Subsequently, the cell lines were exposed to the same panel of second-line treatments in an effort to identify drug combinations that elicit collateral sensitivity. The study found that collateral sensitivity was most often evolved toward etoposide and pemetrexed. Although these drugs had the most optimal response, it was inconsistent, leading to the conclusion that collateral sensitivity is a dynamic state, which is a "moving target" instead of a predictable outcome.

With this understanding, our experiment would, of course, benefit from even more experimental evolutionary replicates to confirm the repeatability of some observations. For example, the evolution of collateral resistance to dactinomycin in all four A673 experimental replicates is consistently stable in the data presented here. However, given the vast genetic contingencies that lead to changes in drug response, observing said stability over many additional replicates would provide a more convincing argument for the consistent evolution of dactinomycin collateral resistance following exposure to VDC/EC.

Performing this experiment in a greater number of cell lines would provide improved insight into the spectrum of responses across various EWS cases. Using increased replicates and additional cell lines would also enhance the analysis of differential gene expression results between responders and non-responders, as we could examine whether differentially expressed genes are consistently dysregulated across different cell lines after exposure to the same experimental conditions. Finally, this work could be improved by examining how collateral drug response in EWS changes during relaxed selection after many drug cycles of the treatment regimen have been applied (Card et al., 2019). This would represent a model that is even more consistent with refractory EWS in a clinical setting, as patients will often have a gap between the initial standard treatment and the selection of second-line treatments.

Despite these caveats, this work provides valuable insight into the evolution of collateral resistance and sensitivity in EWS throughout exposure to standard treatment. Although many studies have examined the role that collateral sensitivity and resistance play in therapeutic response, they frequently ignore intermediate time points during the development of resistance to a primary treatment. In this work, we aimed to examine collateral sensitivity and resistance across time during development of therapeutic resistance to EWS standard of care. We believe this is the first temporal map of collateral sensitivity and resistance in a solid tumor cell line. Using this map, we can see that the path toward collateral sensitivity or resistance is not always straight. Likewise, evolutionary replicates can demonstrate varying collateral drug responses through time, even if their drug response near the end of the experiment is similar. Gene expression signatures can provide clarity when choosing a new treatment in the setting of a tumultuous trajectory toward the evolution of collateral sensitivity or resistance.

Genes with ↑ Expression in SP-Sensitive State			
ALX1	AMZ2	APOBEC3C	ARHGEF6
CD63	DCN	FAM72D	FAM92A
HIST1H1T	IL33	IRX3	LINC00326
LITAF	LYN	MRPS18C	NPIPA5
NRG1	PCSK6	PTGR1	PYCARD
RTN	SP100	SSTR1	TMEM192
TSPAN5	YAF2	ZFAND1	ZNF277
Genes with ↑Expression in SP-Resistant State			
ADGRL2	ANKS6	AP3B2	AP5Z1
ARHGEF9	C7	CAMKV	CCAR2
CD24	CDH4	CHGA	CORO7
CRMP1	DGCR8	DHCR7	DPP3
EPHA4	FASN	FOXO3B	FRG2FP
GALNS	HBA2	HDAC10	INCENP
INTS1	KSR1	LIN28B	LINC01089
LRCH2	MAN2C1	MEG3	MEG8
MRGPRF	MRNIP	MSRA	NEB
NEFM	NOM1	NUP210	PBX1
PC	PCBP2-OT1	PCDH17	PLXNB1
PPP1R1B	PRRC2B	PTPRG-AS1	PPYGO1
RNF130	RNF44	SBNO2	SCAMP4
SCARA3	SLC16A7	SLC29A2	SLITRK3
SYK	TAF15	TAF1C	TAF6L
TMEM271	TUBB3	VAX1	WDR17
WDR27	ZNF354C	ZNF414	ZNF667
ZNF667-AS1	ZNF675	ZNF730	ZNF736

Table 3. Genes with Significant Differential Expression between SP-Resistant and SP-Sensitive Samples
Differential gene expression analysis was performed using EBSeq in R, with maxround set to 15 and FDR of 0.05.

Limitations of the Study

Our experiment would benefit from even more experimental evolutionary replicates to confirm the repeatability of some observations. For example, the evolution of collateral resistance to dactinomycin in all four A673 experimental replicates is consistently stable in the data presented here. However, given the vast genetic contingencies that lead to changes in drug response, observing said stability over many additional replicates would provide a more convincing argument for the consistent evolution of dactinomycin collateral resistance following exposure to VDC/EC. Performing this experiment in a greater number of cell lines would provide improved insight into the spectrum of responses across various EWS cases. Using increased replicates and additional cell lines would also enhance the analysis of differential gene expression results between responders and non-responders, as we could examine whether differentially expressed genes are consistently dysregulated across different cell lines after exposure to the same experimental conditions. Finally, this work could be improved by examining how collateral drug response in EWS changes during relaxed selection after many drug cycles of the treatment regimen have been applied (Card et al., 2019).

This would represent a model that is even more consistent with refractory EWS in a clinical setting, as patients will often have a gap between the initial standard treatment and the selection of second-line treatments.

Resource Availability

Lead Contact

Jacob Scott is the lead contact for this manuscript. He can be reached at scottj10@ccf.org.

Materials Availability

We are glad to share A673 cell line and its resistant derivatives generated in this study with a completed MTA.

Data and Code Availability

The accession number for the sequence data reported in this paper is Sequence Read Archive: PRJNA630293. Original drug response data from the long-term evolution experiments may be accessed through Mendeley Data: https://doi.org/10.17632/vbc3gjjgyn.1. The code to perform all analyses is available via GitHub at https://github.com/jessicascarborough/ES-CS-evolution.

METHODS

All methods can be found in the accompanying Transparent Methods supplemental file.

SUPPLEMENTAL INFORMATION

Supplemental Information can be found online at https://doi.org/10.1016/j.isci.2020.101293.

ACKNOWLEDGMENTS

J.G.S. would like to thank the NIH Loan Repayment Program for their generous support, the Paul Calabresi Career Development Award for Clinical Oncology (NIH K12CA076917), the Carson Sarcoma Foundation, and Chemowarrior Foundation. Additionally, J.A.S. thanks the NIH for support through the T32GM007250 grant. The authors thank the Lerner Research Institute Genomic Core for RNA-sequencing and Kathleen Pishas for helpful discussions and for sharing the cell lines.

AUTHOR CONTRIBUTIONS

J.A.S. performed data processing, wrote all associated code, analyzed the data, and wrote the manuscript. E.M. and M.H. performed the long-term evolution experiments, drug sensitivity assays, and RNA extraction and wrote the manuscript. A. Dhawan contributed to experimental design and analyzed the data. A. Durmaz performed RNA sequencing quality control and alignment. P.A. contributed to experimental design and analyzed the data. J.G.S. analyzed the data and wrote the manuscript.

DECLARATION OF INTERESTS

Stephen Lessnick serves as a Scientific Advisor for Salarius Pharmaceuticals.

Received: February 12, 2020
Revised: May 6, 2020
Accepted: June 15, 2020
Published: July 24, 2020

REFERENCES

Ahmed, A.A., Zia, H., and Wagner, L. (2014). Therapy resistance mechanisms in Ewing's sarcoma family tumors. Cancer Chemother. Pharmacol. *73*, 657–663.

Card, K.J., LaBar, T., Gomez, J.B., and Lenski, R.E. (2019). Historical contingency in the evolution of antibiotic resistance after decades of relaxed selection. PLoS Biol. *17*, e3000397.

Chen, K.G., and Sikic, B.I. (2012). Molecular pathways: regulation and therapeutic implications of multidrug resistance. Clin. Cancer Res. *18*, 1863–1869.

Dhawan, A., Nichol, D., Kinose, F., Abazeed, M.E., Marusyk, A., Haura, E.B., and Scott, J.G. (2017). Collateral sensitivity networks reveal evolutionary instability and novel treatment strategies in alk mutated non-small cell lung cancer. Sci. Rep. *7*, 1–9.

Esiashvili, N., Goodman, M., and Marcus, R.B. (2008). Changes in incidence and survival of Ewing sarcoma patients over the past 3 decades: surveillance epidemiology and end results data. J. Pediatr. Hematol. Oncol. *30*, 425–430.

Fleming, R.A. (1997). An overview of cyclophosphamide and ifosfamide pharmacology. Pharmacother. J. Hum. Pharmacol. Drug Ther. *17*, 146S–154S.

Gatti, L., Sevko, A., De Cesare, M., Arrighetti, N., Manenti, G., Ciusani, E., Verderio, P., Ciniselli, C.M., Cominetti, D., Carenini, N., et al. (2014). Histone deacetylase inhibitor-temozolomide co-treatment inhibits melanoma growth through suppression of chemokine (cc motif) ligand 2-driven signals. Oncotarget *5*, 4516.

Grier, H.E., Krailo, M.D., Tarbell, N.J., Link, M.P., Fryer, C.J., Pritchard, D.J., Gebhardt, M.C., Dickman, P.S., Perlman, E.J., Meyers, P.A., et al. (2003). Addition of ifosfamide and etoposide to standard chemotherapy for Ewing's sarcoma and primitive neuroectodermal tumor of bone. N. Engl. J. Med. *348*, 694–701.

Hall, M.D., Handley, M.D., and Gottesman, M.M. (2009). Is resistance useless? multidrug resistance and collateral sensitivity. Trends Pharmacol. Sci. *30*, 546–556.

Hampsey, M., and Reinberg, D. (1997). Transcription: why are tafs essential? Curr. Biol. *7*, R44–R46.

Huang, M., and Lucas, K. (2010). Current therapeutic approaches in metastatic and recurrent Ewing Sarcoma. Sarcoma *2011*, 863210.

Hunold, A., Weddeling, N., Paulussen, M., Ranft, A., Liebscher, C., and Jürgens, H. (2006). Topotecan and cyclophosphamide in patients with refractory or relapsed Ewing tumors. Pediatr. Blood Cancer *47*, 795–800.

Imamovic, L., and Sommer, M.O. (2013). Use of collateral sensitivity networks to design drug cycling protocols that avoid resistance development. Sci. Transl. Med. *5*, 204ra132.

Klug, A. (1999). Zinc finger peptides for the regulation of gene expression. J. Mol. Biol. *293*, 215–218.

Maltas, J., and Wood, K.B. (2019). Pervasive and diverse collateral sensitivity profiles inform optimal strategies to limit antibiotic resistance. PLoS Biol. *17*, e3000515.

Martınez-Ramırez, A., Rodrıguez-Perales, S., Meléndez, B., Martınez-Delgado, B., Urioste, M., Cigudosa, J., and Benıtez, J. (2003). Characterization of the a673 cell line (Ewing tumor) by molecular cytogenetic techniques. Cancer Genet. Cytogenet. *141*, 138–142.

Munck, C., Gumpert, H.K., Wallin, A.I.N., Wang, H.H., and Sommer, M.O. (2014). Prediction of resistance development against drug combinations by collateral responses to component drugs. Sci. Transl. Med. *6*, 262ra156.

Nichol, D., Jeavons, P., Fletcher, A.G., Bonomo, R.A., Maini, P.K., Paul, J.L., Gatenby, R.A., Anderson, A.R., and Scott, J.G. (2015). Steering evolution with sequential therapy to prevent the emergence of bacterial antibiotic resistance. PLoS Comput. Biol. *11*, e1004493.

Nichol, D., Rutter, J., Bryant, C., Hujer, A.M., Lek, S., Adams, M.D., Jeavons, P., Anderson, A.R., Bonomo, R.A., and Scott, J.G. (2019). Antibiotic collateral sensitivity is contingent on the repeatability of evolution. Nat. Commun. *10*, 1–10.

O'Leary, N.A., Wright, M.W., Brister, J.R., Ciufo, S., Haddad, D., McVeigh, R., Rajput, B., Robbertse, B., Smith-White, B., Ako-Adjei, D., et al. (2016). Reference sequence (refseq) database at ncbi: current status, taxonomic expansion, and functional annotation. Nucleic Acids Res. *44*, D733–D745.

Pál, C., Papp, B., and Lázár, V. (2015). Collateral sensitivity of antibiotic-resistant microbes. Trends Microbiol. *23*, 401–407.

Pluchino, K.M., Hall, M.D., Goldsborough, A.S., Callaghan, R., and Gottesman, M.M. (2012). Collateral sensitivity as a strategy against cancer multidrug resistance. Drug Resist. Updates *15*, 98–105.

Ries, L.A.G. (1999). Cancer Incidence and Survival Among Children and Adolescents: United States SEER Program, 1975-1995, *99* (National Cancer Institute).

Sankar, S., Theisen, E.R., Bearss, J., Mulvihill, T., Hoffman, L.M., Sorna, V., Beckerle, M.C., Sharma, S., and Lessnick, S.L. (2014). Reversible lsd1 inhibition interferes with global ews/ets transcriptional activity and impedes Ewing sarcoma tumor growth. Clin. Cancer Res. *20*, 4584–4597.

Scott, J., and Marusyk, A. (2017). Somatic clonal evolution: a selection-centric perspective. Biochim. Biophys. Acta *1867*, 139–150.

Szuhai, K., IJszenga, M., Tanke, H.J., Rosenberg, C., and Hogendoorn, P.C. (2006). Molecular cytogenetic characterization of four previously established and two newly established ewing sarcoma cell lines. Cancer Genet. Cytogenet. *166*, 173–179.

Womer, R.B., West, D.C., Krailo, M.D., Dickman, P.S., Pawel, B.R., Grier, H.E., Marcus, K., Sailer, S., Healey, J.H., Dormans, J.P., et al. (2012). Randomized controlled trial of interval-compressed chemotherapy for the treatment of localized Ewing sarcoma: a report from the children's oncology group. J. Clin. Oncol. *30*, 4148.

Yang, G.J., Lei, P.M., Wong, S.Y., Ma, D.L., and Leung, C.H. (2018). Pharmacological inhibition of lsd1 for cancer treatment. Molecules *23*, 3194.

Zhao, B., Sedlak, J.C., Srinivas, R., Creixell, P., Pritchard, J.R., Tidor, B., Lauffenburger, D.A., and Hemann, M.T. (2016). Exploiting temporal collateral sensitivity in tumor clonal evolution. Cell *165*, 234–246.

iScience, Volume *23*

Supplemental Information

Identifying States of Collateral Sensitivity during the Evolution of Therapeutic Resistance in Ewing's Sarcoma

Jessica A. Scarborough, Erin McClure, Peter Anderson, Andrew Dhawan, Arda Durmaz, Stephen L. Lessnick, Masahiro Hitomi, and Jacob G. Scott

Supplementary Information

1. Supplementary Figures and Legends

1.1. Complete A673 EC50 Data

The following plots mirror Figures 2 and 3, respectively. EC50 for Replicate 5 against olaparib at the VDC5 timepoint is not censored, as seen in Figures 2 and 3. Additionally, the drugs removed from main text analysis, vincristine, pazopanib, and sodium thiosulfate are included. These drugs were censored in the main text due to poorly fit dose-response models. Interpretation of these plots can be found in the main text.

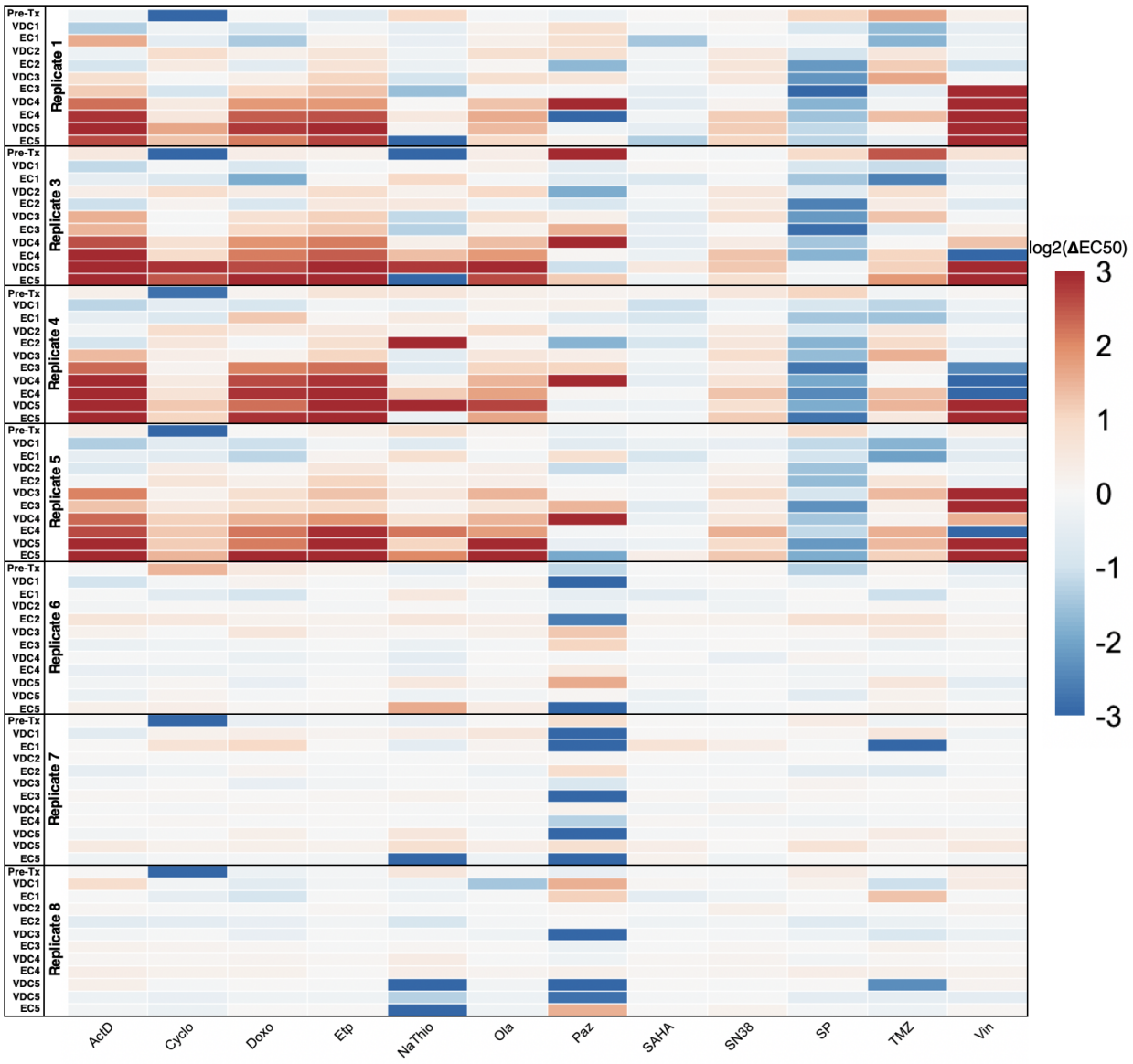

Supplementary Figure 1: **Uncensored temporal collateral sensitivity map representing EC50 changes to panel of drugs in A673 cell line as it develops resistance to standard treatment, related to Figure 2.** A heatmap representing how the EC50 to a panel of nine drugs changes in 4 experimental and 3 control evolutionary replicates from the A673 cell line as they are exposed to the VDC/EC drug combinations over time. Color represents the $\log_2$ fold change of EC50 to a drug (columns) for a replicate at a given evolutionary time point (rows) compared to the average EC50 of the three control evolutionary replicates at the corresponding time point. Time points are denoted as the drug combination that a given replicate has recently recovered from. For example, the data representing dose-response models after the first application of the VDC drug combination would be labeled with VDC1.

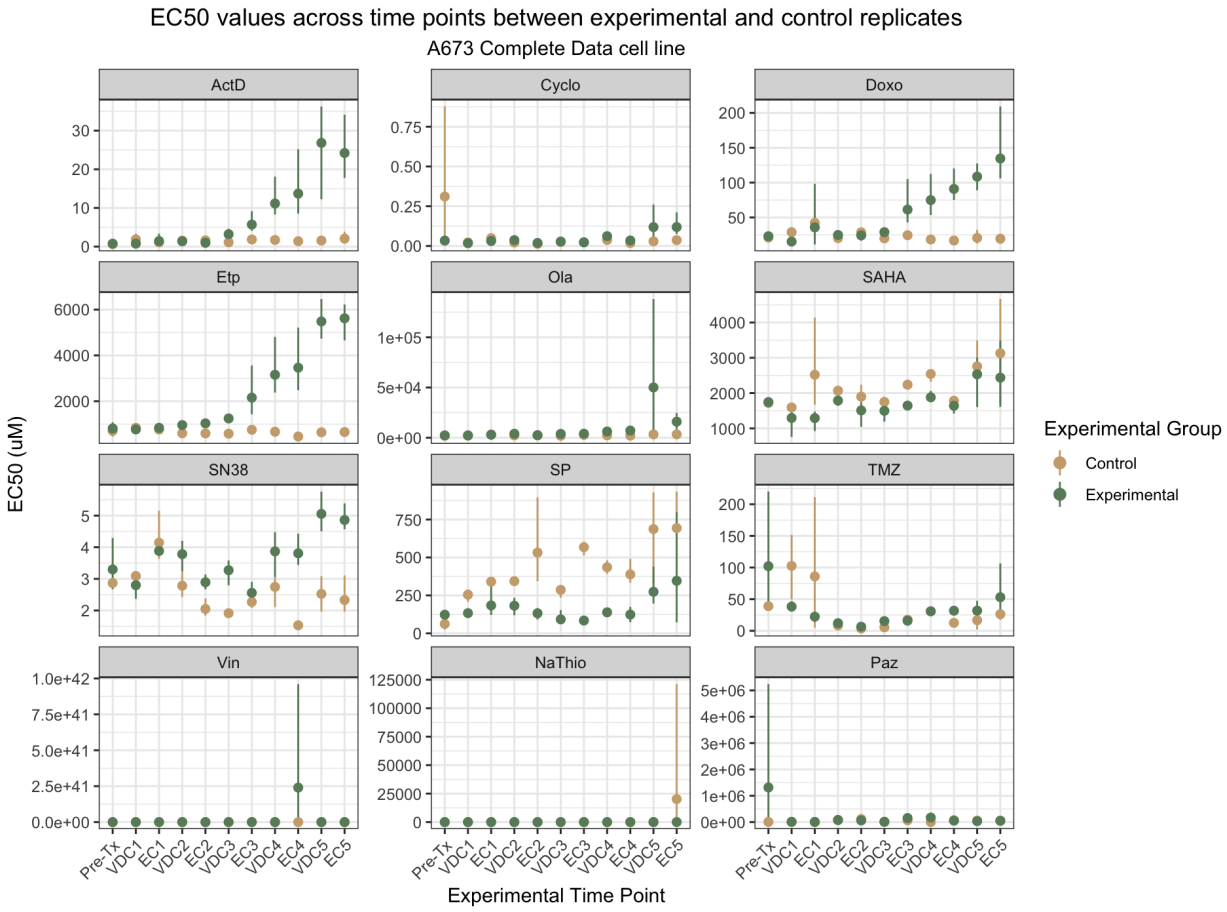

Supplementary Figure 2: **Uncensored point-range plots demonstrating EC50 changes in A673 experimental and control replicates over time, related to Figure 3.** Point-range plots representing the changes in drug response to a panel of 12 drugs. Experimental time points (x-axis) represent which step in the drug cycle the replicates have just recovered from. Points on the plot represent the average EC50 for the group, either experimental or control. Lines represent the range for the entire group. The y-axis of all the point-range plots has uM units, except Cyclo and NaThio, where the units are percent by volume.

1.2. Complete TTC466 EC50 Data

Supplementary Figures 3 and 4 display the changes in drug response to all 12 agents over time in the TTC466 cell line. In comparing the two cell lines, it is clear that the A673 cell line displays more stable behavior, while the TTC466 cell line shows much more variability over time. In other words, as the treatment cycles progress, the A673 cell line tends to move steadily towards a resistant or sensitive state, while the TTC466 cell line tends to fluctuate more. The TTC466 control replicates also tend to have more fluctuation between time points, despite being exposed to only media and having relative agreement between technical replicates. For this reason, we chose to focus our analysis on the A673 cell line, while the TTC466 cell line results can be found in the Supplementary Information.

In Supplementary Figure 3, we see that after the first exposure to the VDC drug combination (VDC1) in the TTC466 cell line, resistance to cyclophosphamide suddenly emerges. This doesn't occur in any other replicate, nor at any other time point. These findings were confirmed by examining the drug-response curve at this time point to ensure a well-fit model. Two hypotheses for why the replicate didn't retain the cyclophosphamide-resistant trait in the next generation include an equally rapid loss of this trait in the next generations or a bottleneck selection during the procedure where the cells that were resistant to cyclophosphamide were not plated for the next round of the drug treatment cycle. Next, another example of drug-response fluctuation in the TTC466 cell line may have been mistaken as a rare shift in drug response if only one evolutionary replicate had been performed. In Supplementary Figure 3, we see that after the second exposure to the EC combination (EC2), the EC50 of every experimental replicate has increased chemoresistance to olaparib before returning to a more sensitive state after the next drug cycle. Supplementary Figure 4, demonstrates that there is a large range in the control replicates at the corresponding time point, which makes the comparison between the experimental and control replicates less reliable; however, it is clear that from the time points before and after EC2, the EC50 increases significantly at EC2.

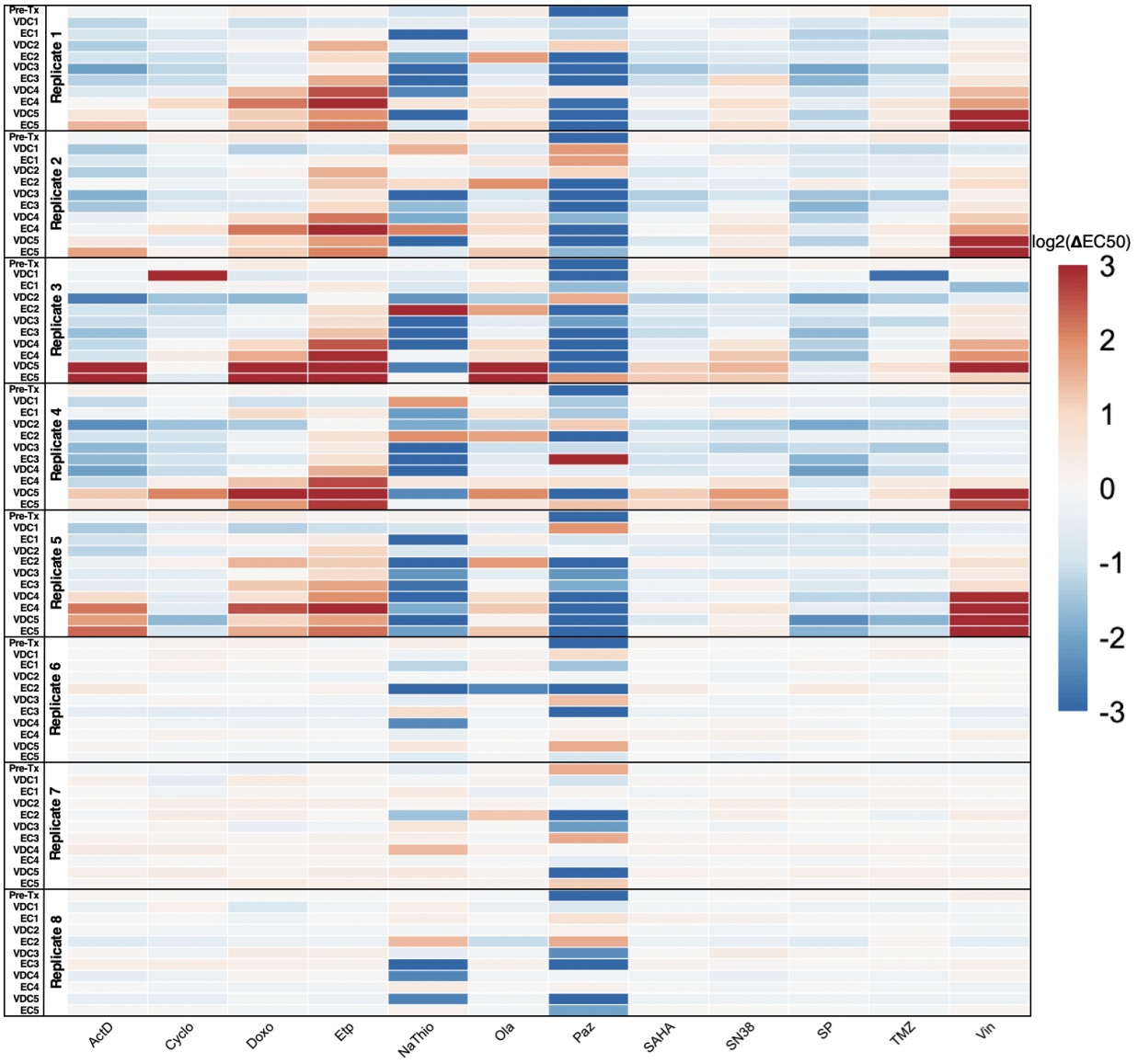

Supplementary Figure 3: **Uncensored temporal collateral sensitivity map representing EC50 changes to panel of drugs in TTC466 cell line as it develops resistance to standard treatment, related to Figure 2.** A heatmap representing how the EC50 to a panel of nine drugs changes in 5 experimental and 3 control evolutionary replicates from the TTC466 cell line as they are exposed to the VDC/EC drug combinations over time. Color represents the $\log_2$ fold change of EC50 to a drug (columns) for a replicate at a given evolutionary time point (rows) compared to the average EC50 of the three control evolutionary replicates at the corresponding time point. Time points are denoted as the drug combination that a given replicate has recently recovered from. For example, the data representing dose-response models after the first application of the VDC drug combination would be labeled with VDC1.

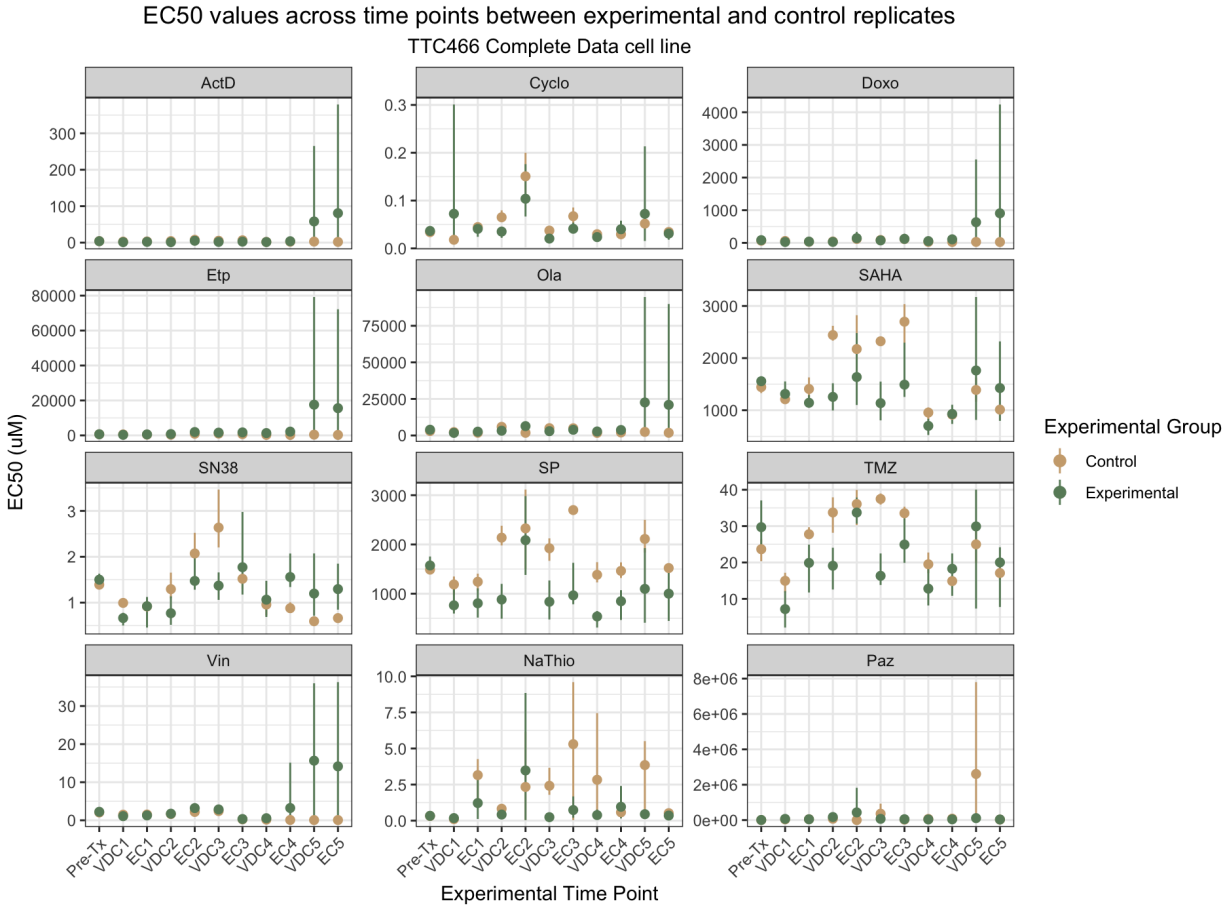

Supplementary Figure 4: **Uncensored point-range plots demonstrating EC50 changes in TTC466 experimental and control replicates over time, related to Figure 3.** Point-range plots representing the changes in drug response to a panel of 12 drugs. Experimental time points (x-axis) represent which step in the drug cycle the replicates have just recovered from. Points on the plot represent the average EC50 for the group, either experimental or control. Lines represent the range for the entire group. The y-axis of all the point-range plots has uM units, except Cyclo and NaThio, where the units are percent by volume.

1.3. Waterfall plots for sequenced samples against all drugs

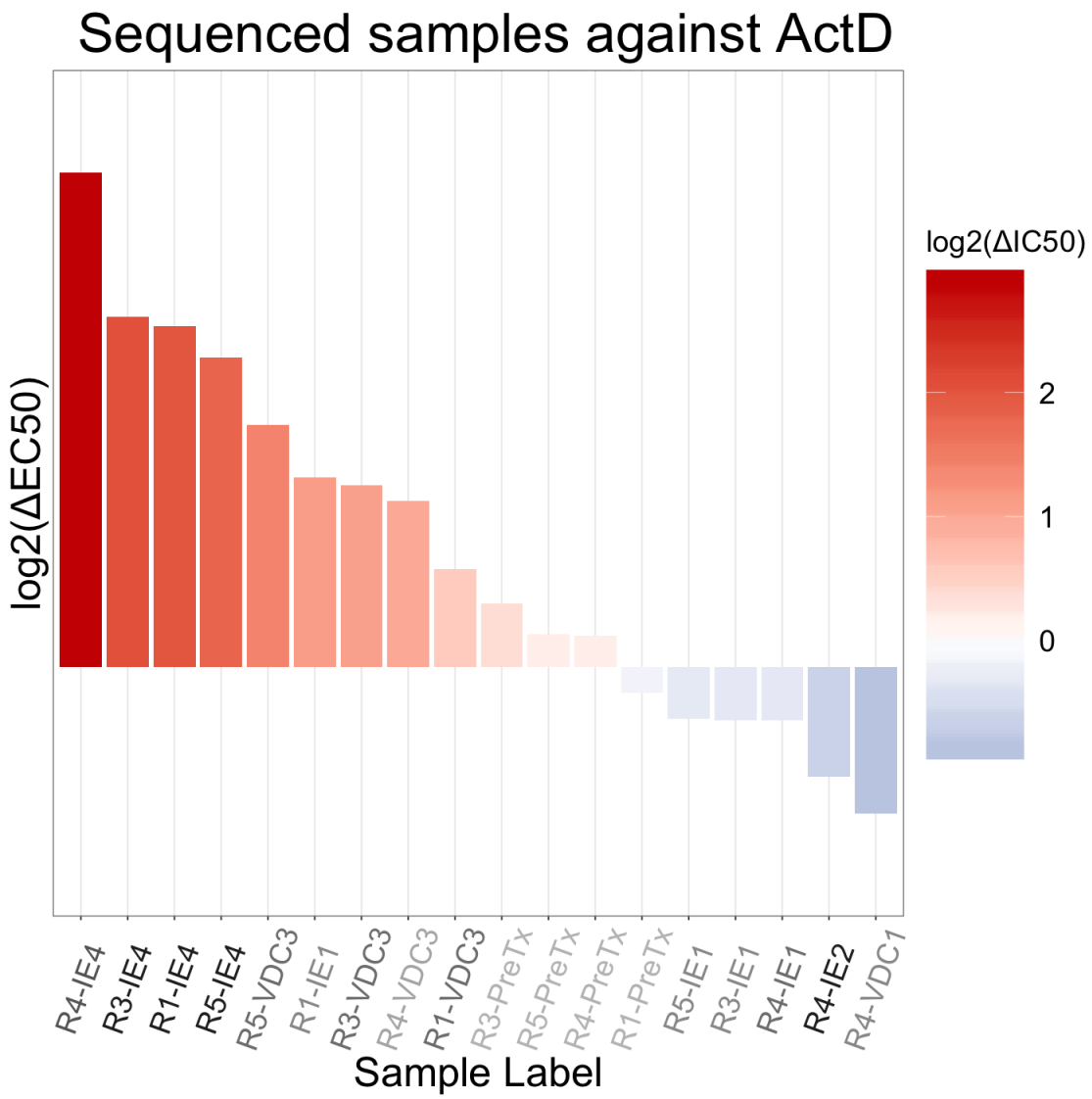

Supplementary Figure 5: **Waterfall of EC50 values for sequenced samples against dactinomycin, related to Figure 4.** Color represents $\log_2$ change in EC50 between the sample and average control EC50 at the given time point. Red shows a change towards resistance, while blue shows a change towards sensitivity. Samples are ranked along the x-axis from least-to-most sensitive. Sample labels on the x-axis are represented by darker colors the longer they have been evolved in the evolutionary experiment.

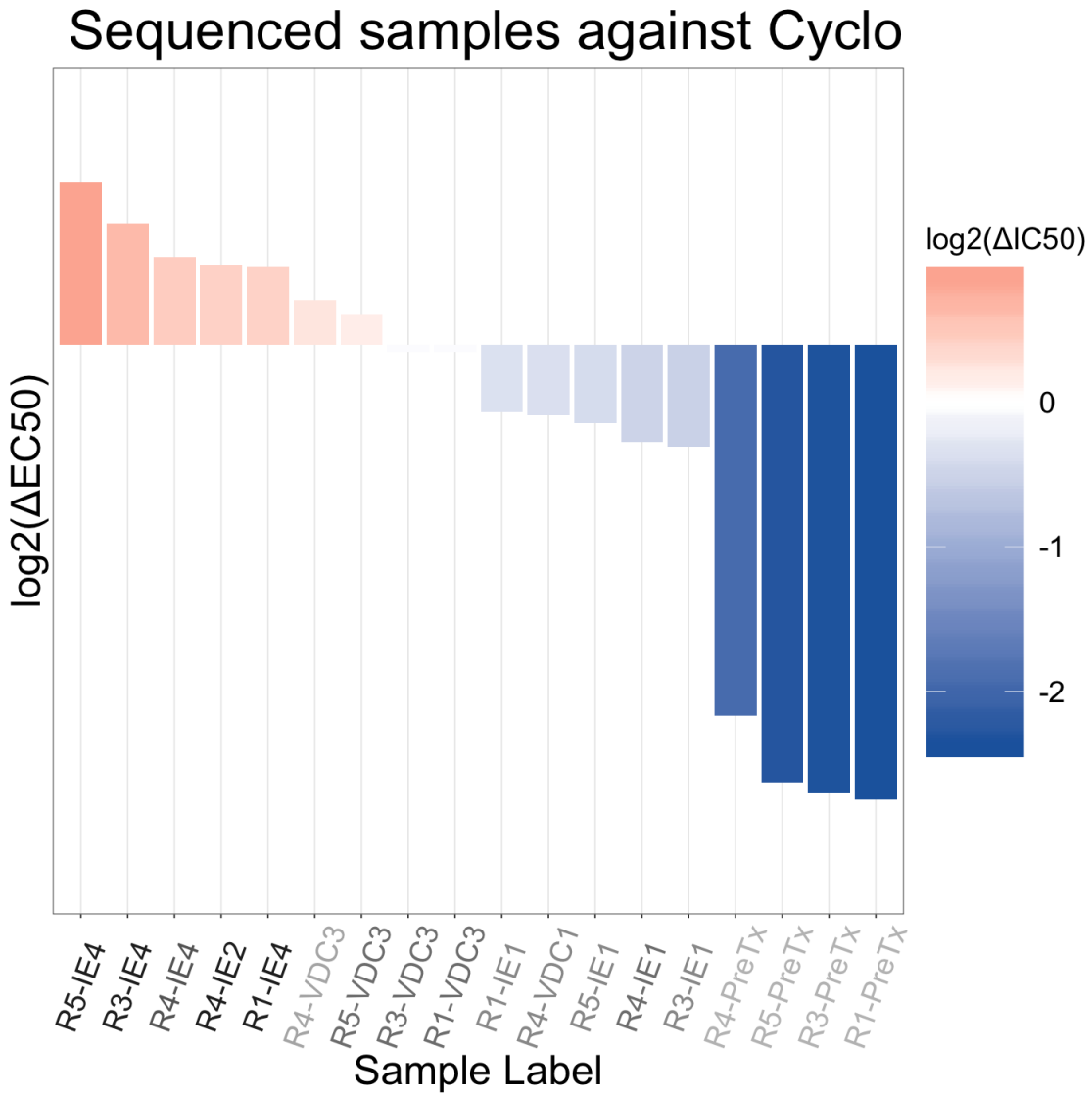

Supplementary Figure 6: **Waterfall of EC50 values for sequenced samples against cyclophosphamide, related to Figure 4.** Color represents $\log_2$ change in EC50 between the sample and average control EC50 at the given time point. Red shows a change towards resistance, while blue shows a change towards sensitivity. Samples are ranked along the x-axis from least-to-most sensitive. Sample labels on the x-axis are represented by darker colors the longer they have been evolved in the evolutionary experiment.

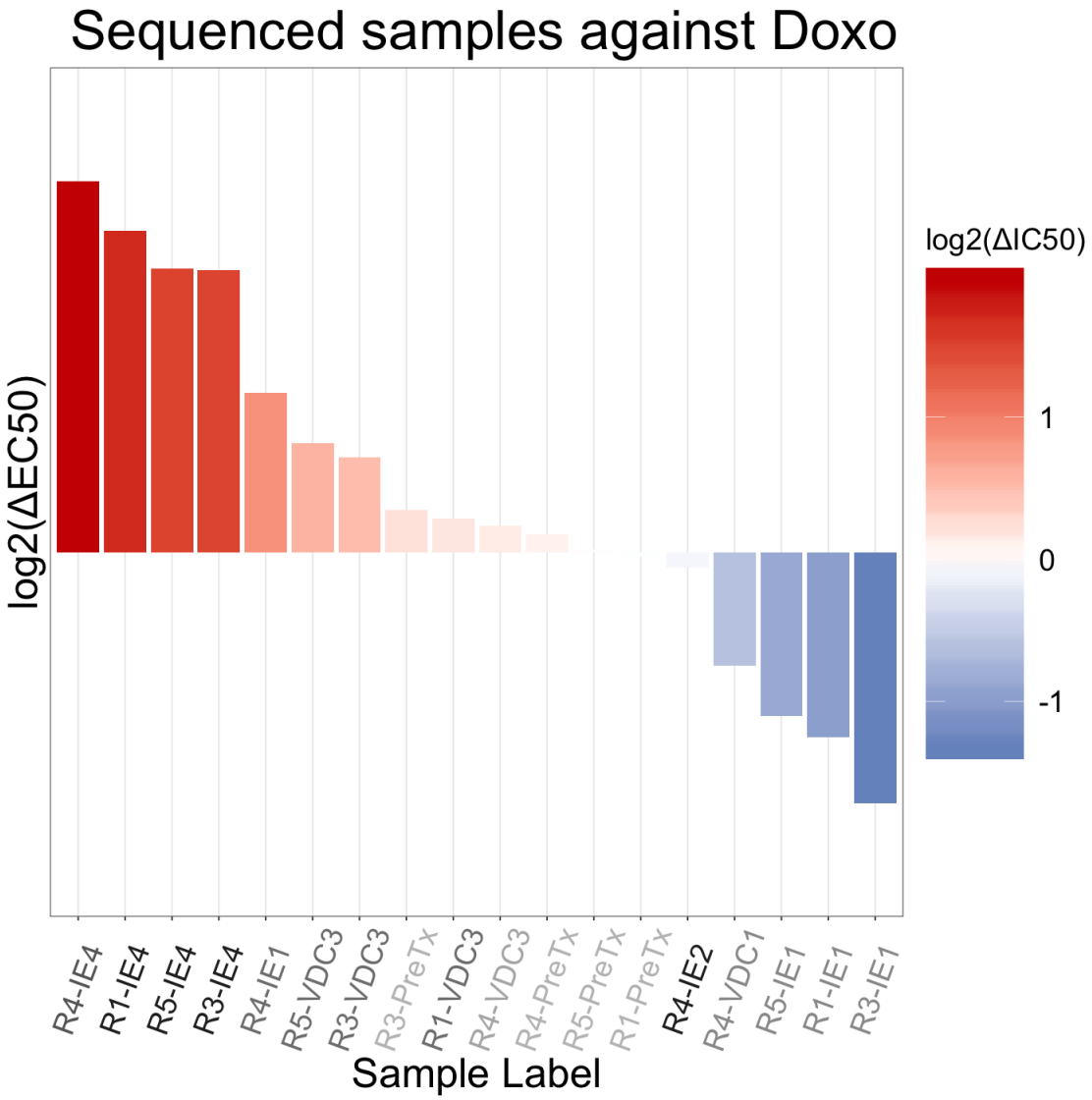

Supplementary Figure 7: **Waterfall of EC50 values for sequenced samples against doxorubicin, related to Figure 4.** Color represents $\log_2$ change in EC50 between the sample and average control EC50 at the given time point. Red shows a change towards resistance, while blue shows a change towards sensitivity. Samples are ranked along the x-axis from least-to-most sensitive. Sample labels on the x-axis are represented by darker colors the longer they have been evolved in the evolutionary experiment.

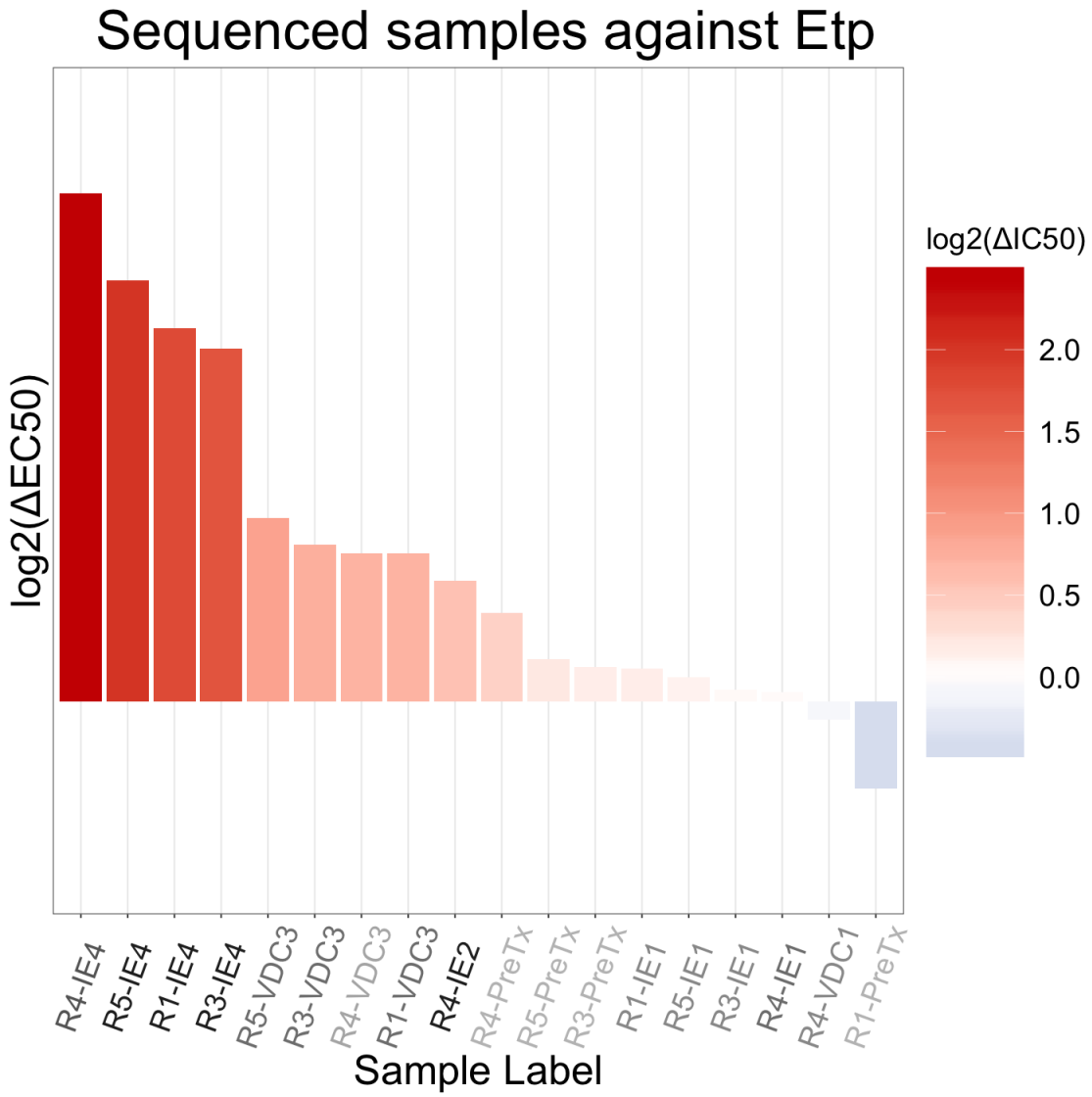

Supplementary Figure 8: **Waterfall of EC50 values for sequenced samples against etoposide, related to Figure 4.** Color represents $\log_2$ change in EC50 between the sample and average control EC50 at the given time point. Red shows a change towards resistance, while blue shows a change towards sensitivity. Samples are ranked along the x-axis from least-to-most sensitive. Sample labels on the x-axis are represented by darker colors the longer they have been evolved in the evolutionary experiment.

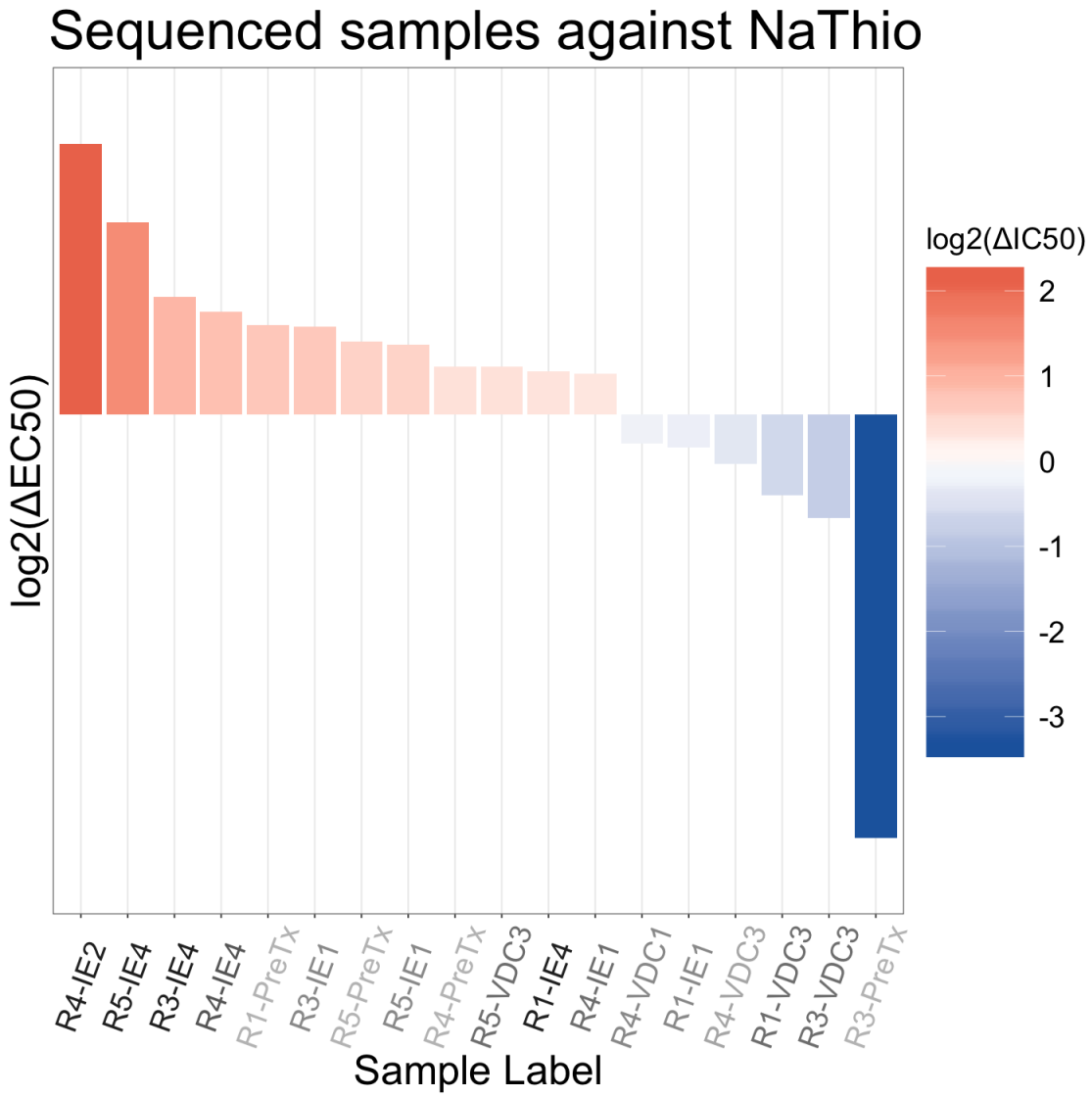

Supplementary Figure 9: **Waterfall of EC50 values for sequenced samples against sodium thiosulfate, related to Figure 4.** Color represents $\log_2$ change in EC50 between the sample and average control EC50 at the given time point. Red shows a change towards resistance, while blue shows a change towards sensitivity. Samples are ranked along the x-axis from least-to-most sensitive. Sample labels on the x-axis are represented by darker colors the longer they have been evolved in the evolutionary experiment.

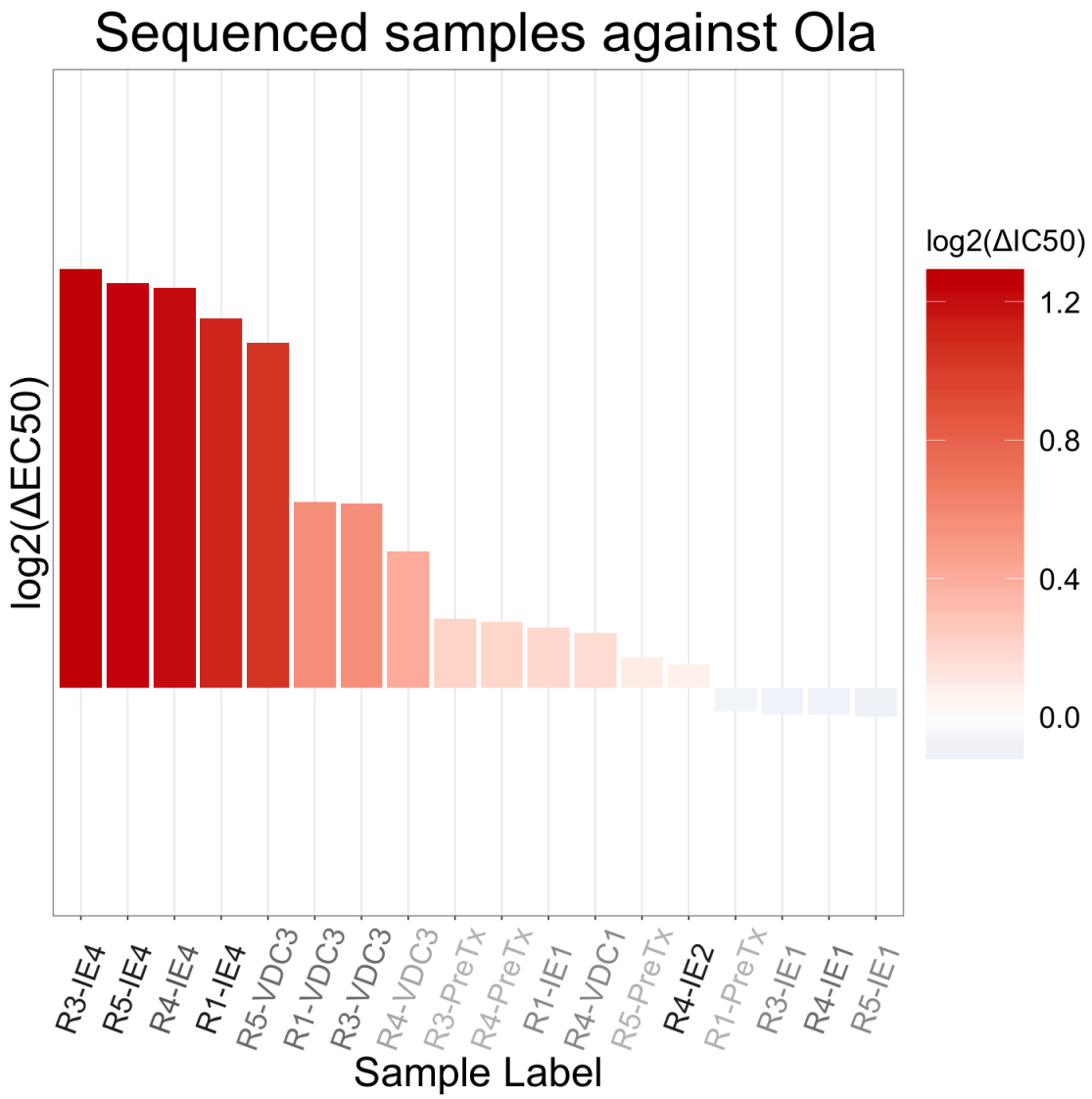

Supplementary Figure 10: **Waterfall of EC50 values for sequenced samples against olaparib, related to Figure 4.** Color represents $\log_2$ change in EC50 between the sample and average control EC50 at the given time point. Red shows a change towards resistance, while blue shows a change towards sensitivity. Samples are ranked along the x-axis from least-to-most sensitive. Sample labels on the x-axis are represented by darker colors the longer they have been evolved in the evolutionary experiment.

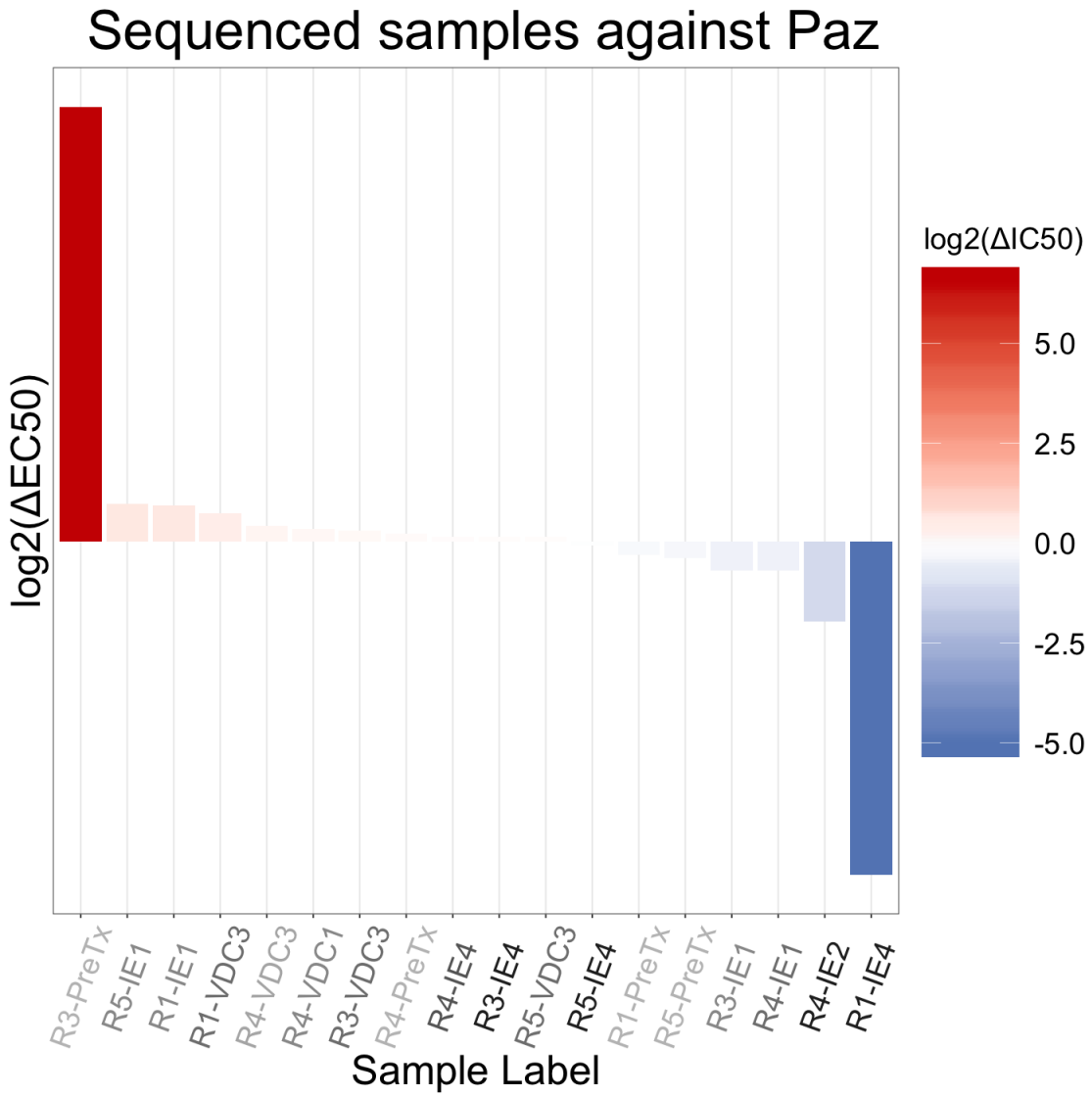

Supplementary Figure 11: **Waterfall of EC50 values for sequenced samples against pazopanib, related to Figure 4.** Color represents $\log_2$ change in EC50 between the sample and average control EC50 at the given time point. Red shows a change towards resistance, while blue shows a change towards sensitivity. Samples are ranked along the x-axis from least-to-most sensitive. Sample labels on the x-axis are represented by darker colors the longer they have been evolved in the evolutionary experiment.

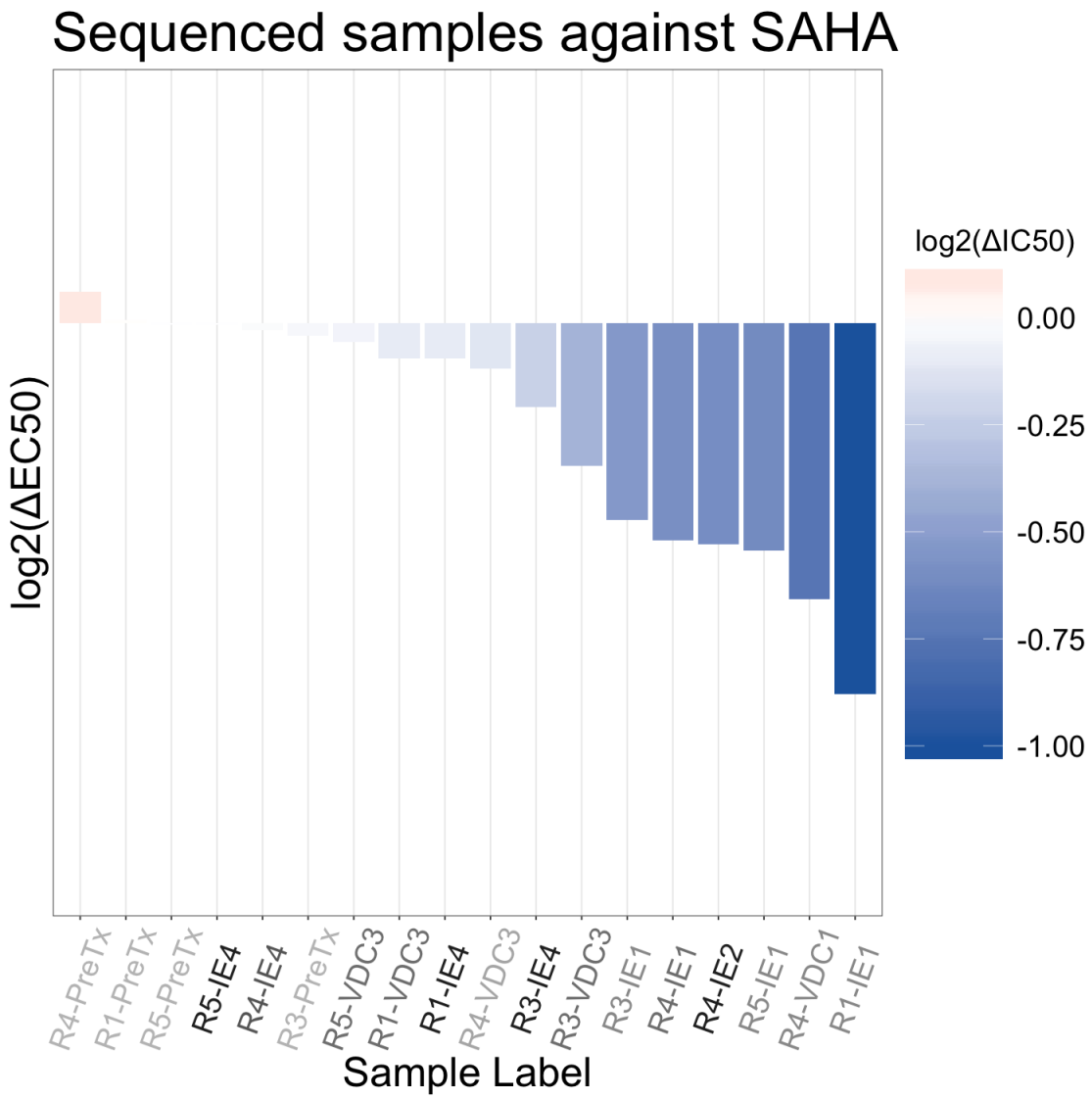

Supplementary Figure 12: **Waterfall of EC50 values for sequenced samples against vorinostat (SAHA), related to Figure 4.** Color represents $\log_2$ change in EC50 between the sample and average control EC50 at the given time point. Red shows a change towards resistance, while blue shows a change towards sensitivity. Samples are ranked along the x-axis from least-to-most sensitive. Sample labels on the x-axis are represented by darker colors the longer they have been evolved in the evolutionary experiment.

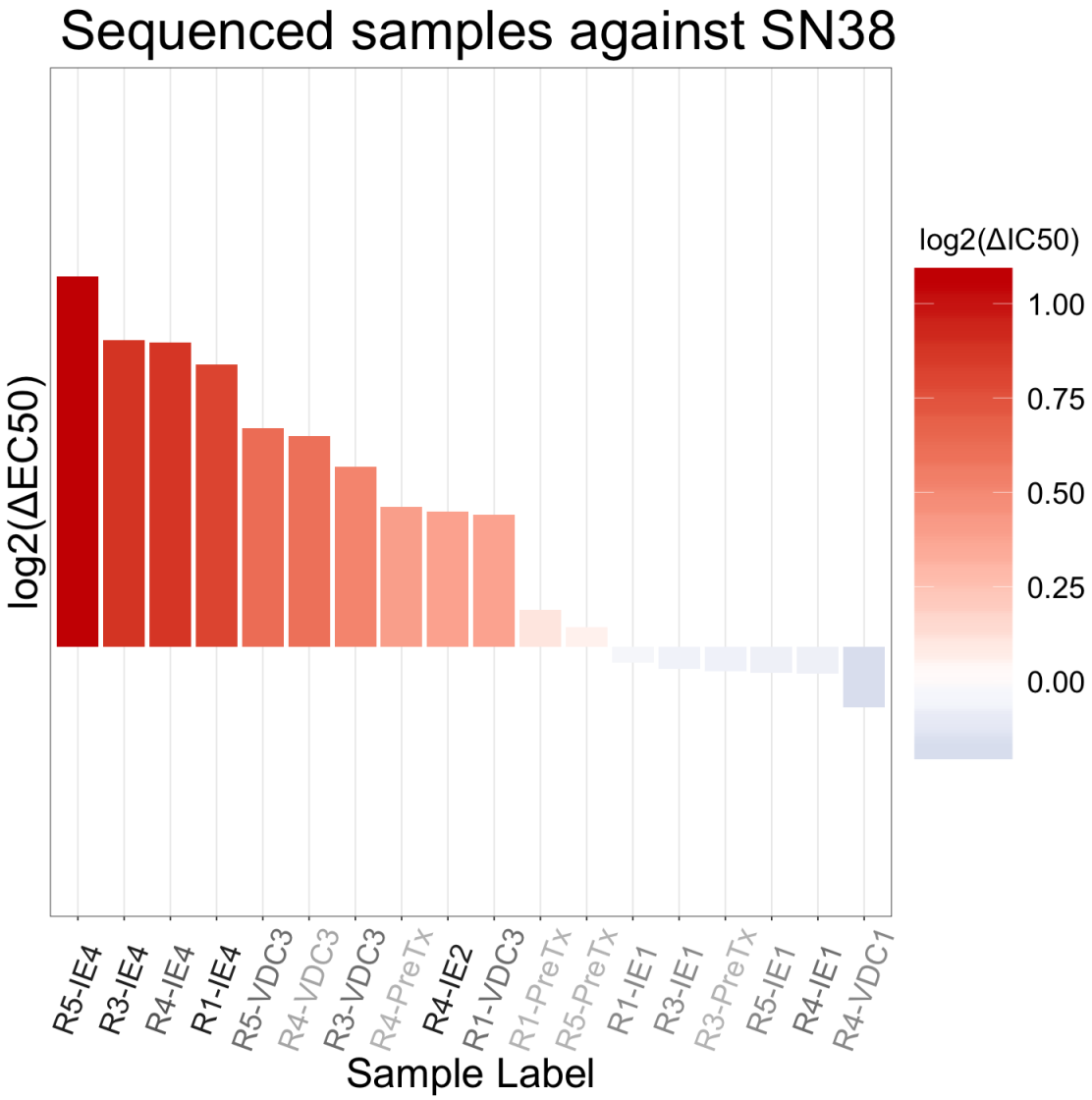

Supplementary Figure 13: **Waterfall of EC50 values for sequenced samples against irinotecan (active metabolite, SN38), related to Figure 4.** Color represents $\log_2$ change in EC50 between the sample and average control EC50 at the given time point. Red shows a change towards resistance, while blue shows a change towards sensitivity. Samples are ranked along the x-axis from least-to-most sensitive. Sample labels on the x-axis are represented by darker colors the longer they have been evolved in the evolutionary experiment.

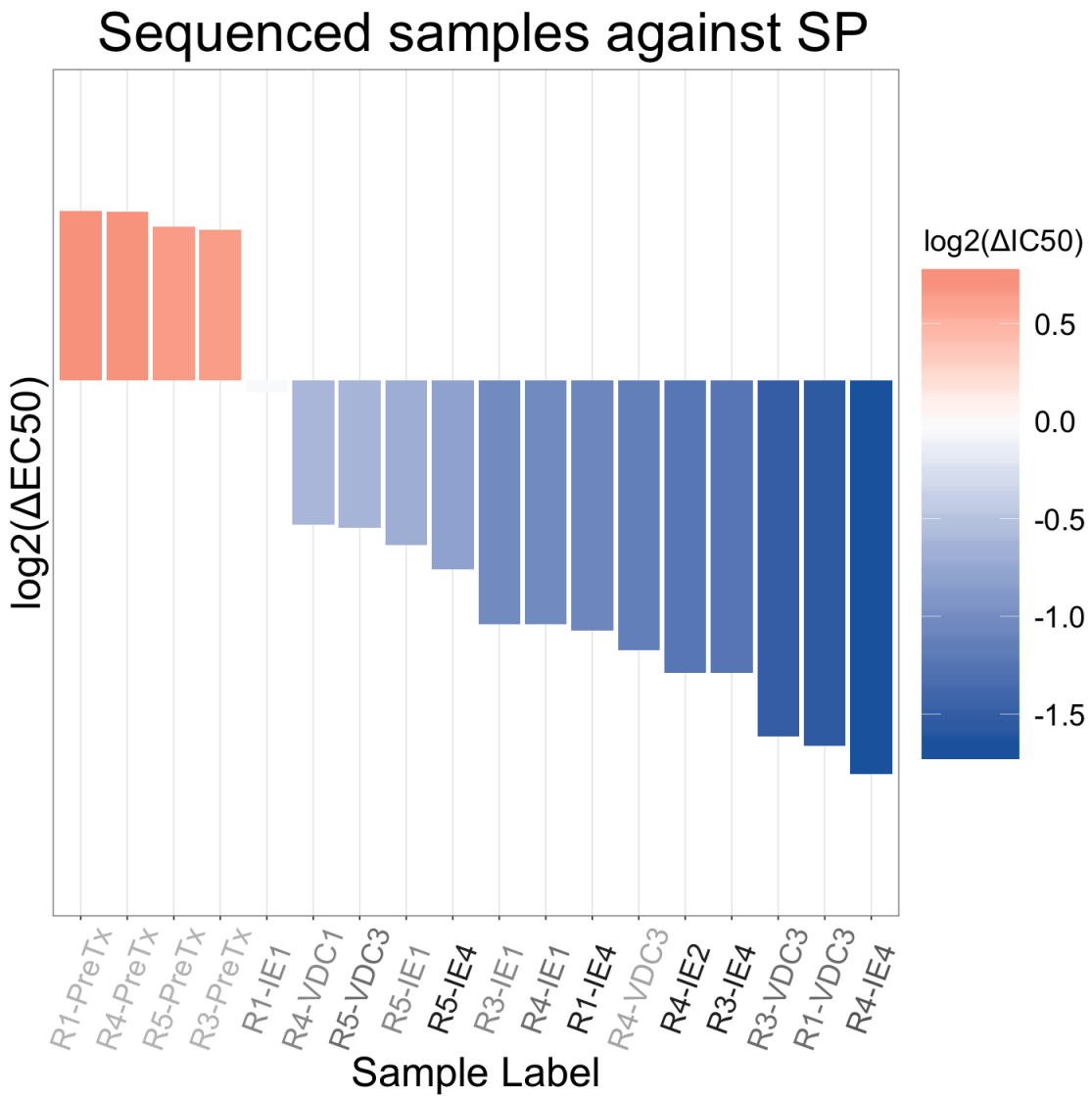

Supplementary Figure 14: **Waterfall of EC50 values for sequenced samples against SP-2509, related to Figure 4.** Color represents $\log_2$ change in EC50 between the sample and average control EC50 at the given time point. Red shows a change towards resistance, while blue shows a change towards sensitivity. Samples are ranked along the x-axis from least-to-most sensitive. Sample labels on the x-axis are represented by darker colors the longer they have been evolved in the evolutionary experiment.

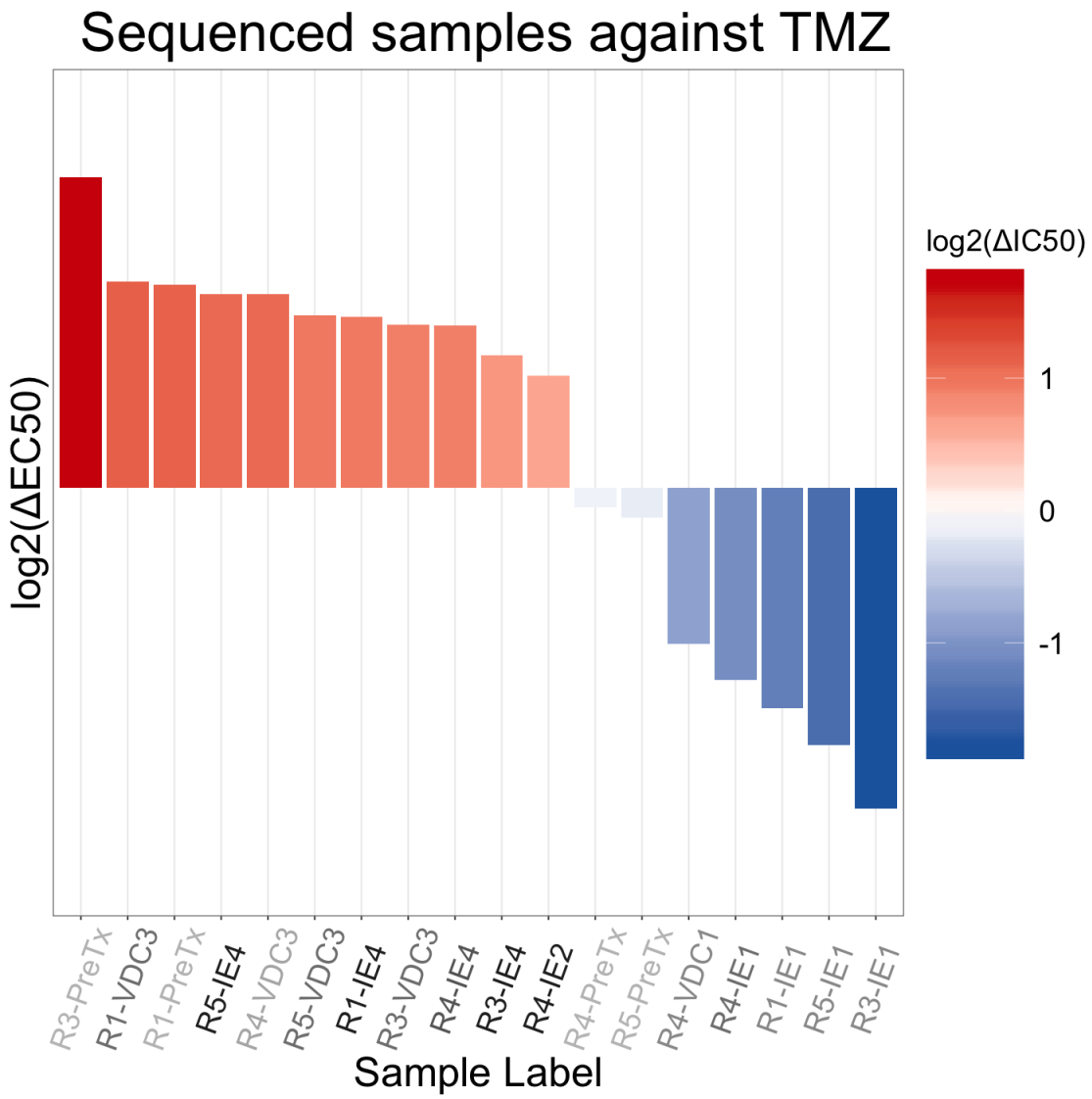

Supplementary Figure 15: **Waterfall of EC50 values for sequenced samples against temozolomide, related to Figure 4.** Color represents $\log_2$ change in EC50 between the sample and average control EC50 at the given time point. Red shows a change towards resistance, while blue shows a change towards sensitivity. Samples are ranked along the x-axis from least-to-most sensitive. Sample labels on the x-axis are represented by darker colors the longer they have been evolved in the evolutionary experiment.

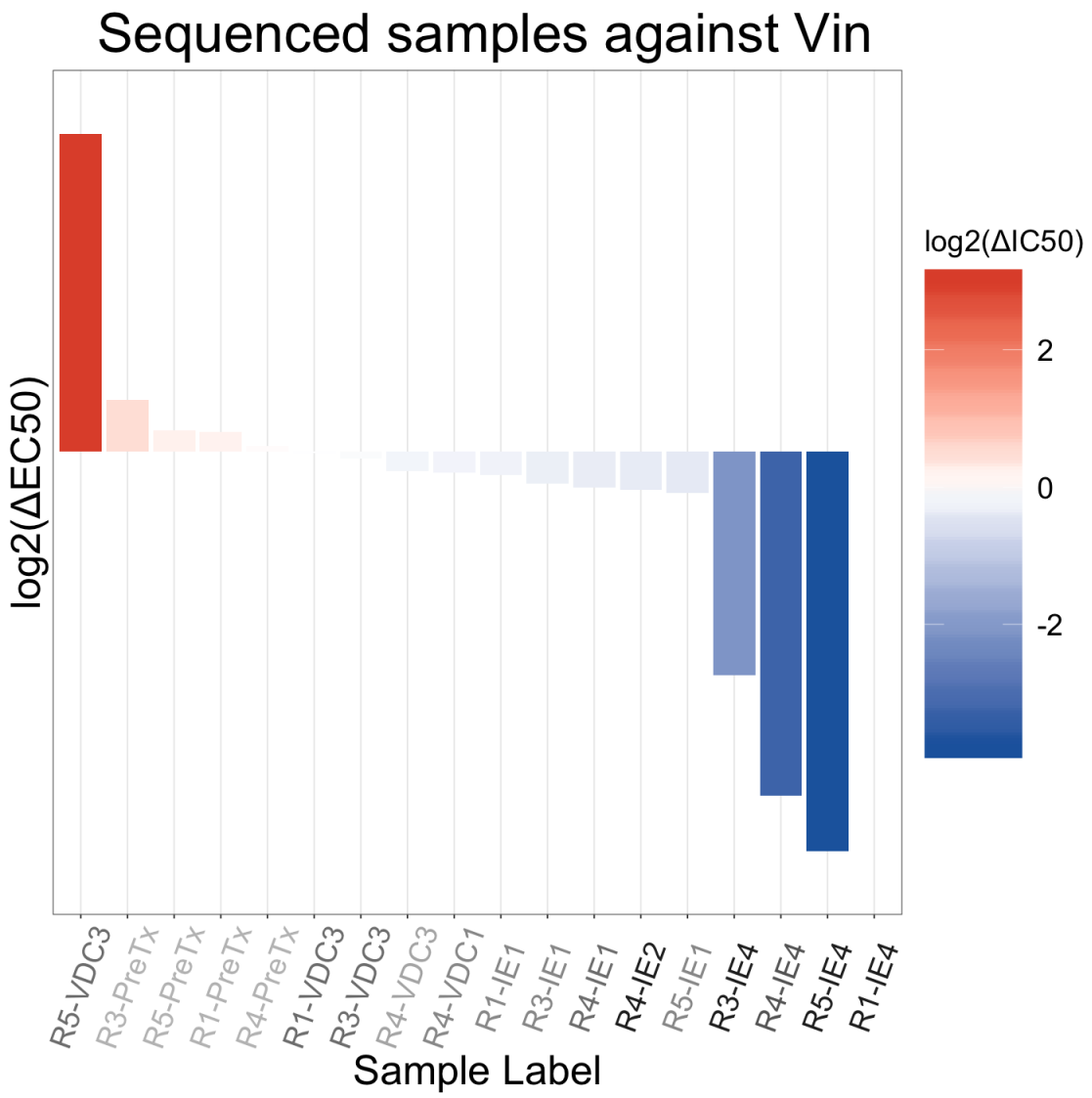

Supplementary Figure 16: **Waterfall of EC50 values for sequenced samples against vincristine, related to Figure 4.** Color represents $\log_2$ change in EC50 between the sample and average control EC50 at the given time point. Red shows a change towards resistance, while blue shows a change towards sensitivity. Samples are ranked along the x-axis from least-to-most sensitive. Sample labels on the x-axis are represented by darker colors the longer they have been evolved in the evolutionary experiment. The EC50 for the first replicate after the fourth exposure to the EC drug combination (R1-EC4) was indeterminant and removed from the waterfall plot.

2. Transparent Methods

Materials

EWS cells (A673 and TTC466 cells) were generous gifts from Dr. Stephen Lessnick at Nationwide Children's Hospital, Columbus, OH.

4-hydroperoxycyclophosphamide and sodium thiosulfate were purchased from Toronto Research Chemicals (North York, ON, Canada). Dactinomycin, SP-2509, doxorubicin, etoposide, temozolomide, pazopanib, olaparib, SAHA, and vincristine were products of Cayman Chemical (Ann Abor, MI). SN-38 was obtained from SelleckChem.com (Houston, TX). The classifications and abbreviations used for all these compounds are found in Table 1.

Cell culture

A673 cells were maintained in Dulbecco's Modified Eagle Medium (D-MEM) supplemented with 10% Fetal Bovine Serum (FBS) and penicillin and streptomycin at 37°C under humidified atmosphere containing 5% CO2. TTC466 cells were cultured in the same way except Roswell Park Memorial Institute (RPMI) medium was used instead of D-MEM.

In vitro combination drug treatments to induce drug resistance

Through drug toxicity assays, we determined EC50 concentrations of chemotherapeutics that are used as standard-of-care to treat EWS (Grier et al., 2003). This standard-of-care treatment for EWS consists of a vincristine-doxorubicin-cyclophosphamide (VDC) combination cycle followed by an etoposide-ifosfamide (EI) combination cycle. However, both cyclophosphamide and ifosfamide are prodrugs, requiring metabolic activation by an *in vivo* model. In the VDC drug combination, cyclophosphamide is replaced by 4-hydroxycyclophosphamide, an activated form of cyclophosphamide; however, there is no such commercially available option for ifosfamide. As ifosfamide is an analog of cyclophosphamide, it was also replaced by 4-hydroperoxycyclophosphamide, due to their similar chemical structures and mechanisms of action. Therefore, we recapitulate Ewing's sarcoma standard-of-care treatment regimen *in vitro* by cycling vincristine-doxorubicin-4-hydroxycyclophosphamide (VDC) and etoposide-4-hydroxycyclophosphamide (EC). The EC50 values were vincristine (0.8 and 0.9 nM), doxorubicin (0.015 and 0.023 nM), 4-hydroxycyclophosphamide (0.001 and 0.001 % by volume), and etoposide (0.7 and 0.37 μM) in the A673 and TTC466 cell lines, respectively.

In order to induce drug resistance in the A673 and TTC466 cell lines, each cell line was plated as 8 biological (evolutionary) replicates, where 5 experimental replicates were exposed to the drug combination cycles, described below, and 3 control replicates were maintained in dimethyl sulfoxide (DMSO). Due to contamination, one of the experimental replicates (Replicate 2) in the A673 cell line was discontinued. Experimental replicates were exposed to the standard-of-care drug cycles, as illustrated in Figure 1. Cells (2×10^6 cells/10cm plate) were first exposed to a combination of vincristine, doxorubicin, and 4-hydroxycyclophosphamide at their EC50 concentrations. After 5 days of incubation, the medium was changed to maintenance medium without drugs. After they proliferate to sub-confluent density, a 10 cm plate was set for the next cycle with etoposide and 4-hydroxycyclophosphamide at their initial EC50 concentrations for 5 days, 96-well plates were set for drug sensitivity assay, and a fraction of cells were snap frozen for RNA extraction. Again, as the treated cultures grew to sub-confluence, this cycle was repeated with alternate exposure to the two drug combinations, along with drug sensitivity assays and sampling for RNA extraction between each drug cycle. On the fifth application of the VDC drug combination, the concentration of the drug combination was increased to 6 nM, 0.05 mM, and 0.006% by volume for vincristine, doxorubicin, and cyclophosphamide, respectively.

Drug toxicity assay

Cells were plated into 96-well plates at the density of 6,000 cells/90μl/well. The next day, 10 μl of medium containing various concentrations of drug of interest were added to each well. The final concentration of

DMSO used as solvent was kept constant (0.1% by volume for dactinomycin, SP2509, doxorubicin, etoposide, olaparib, SAHA, SN38, and vincristine; and 1% by volume for temozolomide and pazopanib).

4-hydroxycyclophosphamide was prepared freshly just prior to each assay by incubating 1 mg of 4-hydroperoxycyclophosphamide with 100 μL of water containing 1 mg sodium thiosulfate at room temperature for 30 sec, converting 4-hydroperoxycyclophosphamide to 4-hydroxycyclophosphamide. The resulting solution was used for toxicity assay starting with 0.2% (by volume) as the highest concentration. Matching dilution series of sodium thiosulfate solution was assessed as a control to assess 4-hydroxycyclophosphamide toxicity, again using 0.2% (by volume) as the highest concentration.

After five days of incubation, cell viability of each well was determined by measuring the enzymatic conversion of alamarBlue (Bio-Rad, Hercles, CA) (Hamid et al., 2004). After addition of alamarBlue solution (10 μl/well), the plate was incubated for two to four hours and the fluorescence intensity (excitation 560 nm / emission 590 nm) of each well was detected by Symphony H2(BioTek, Winooski, VT), a multi-well plate reader. Background fluorescence was determined by measuring the wells without cells incubated with alamarBlue.

Drug response modeling and EC50 estimation

Net alamarBlue conversion for each well was calculated by subtracting the average background fluorescence from each of the fluorescence values. A four-parameter log-logistic (LL.4) model (Hill function) was fit for each biological replicate, performed in triplicate, using the drm function from the drc package in R. This function models the survival measure $S(X)$ at a given dose X as:

$$S(X) = b + \frac{a - b}{1 + \left(\frac{EC50}{X}\right)^H}$$

where $S(X)$ is the expected response at dose X, a is the minimum response (when dose = 0), b is the highest response (when dose = ∞), $EC50$ is the point of inflection (dose at which 50% of the response occurs), and H (known as the Hill slope) is the steepest part of the curve (Gadagkar and Call, 2015). A negative value for H, as seen in these models, denotes a descending curve, while a positive H represents an ascending curve. Estimated EC50 from these models was solved using the ED function from the drc package (version 3.0.1) in R.

Although there is no perfect measure of drug sensitivity and resistance, we chose EC50 as our measure of drug response, because of its compatibility with existing literature and because of the agreement of this model to experimental data. A caveat of this measure is the possibility for the maximum response, b changes, while the point of inflection, $EC50$, for the curve does not (Jang et al., 2014). A plot of all dose-response triplicates with their estimated EC50 can be found in the linked GitHub repository.

RNA extraction and sequencing

Ribosomal-RNA depleted RNA was prepared from 18 samples of interest using RiboMinus Eukaryote Kit (ThermoFisher, Waltham, MA). RNA sequencing was performed at the Genomic Core, the Lerner Research Institute (Cleveland, OH) with HiSeq 2500 (Illumina, San Diego, CA). Quality control and read trimming was performed using fastp v0.20.0 (Chen et al., 2018). Read alignment was done using STAR v2.7.1 and alignment quantification was done using salmon v0.14.1 against gencode v31 transcript set with average 12 million reads per sample (Dobin et al., 2013; Patro et al., 2017; Harrow et al., 2012). Transcript level abundance estimates were then converted to gene level estimated counts using tximport R package (Soneson et al., 2015).

Differential gene expression analysis

Samples sent for sequencing were ranked based on their EC50 to each drug. For each drug analyzed, differential gene expression (DE) analysis compared samples in the top and bottom third of the ranked EC50 values. This DE analysis was performed using the EBSeq R package (version 1.24.0), with a false discovery threshold of 0.05 and the maxround parameter set to 15 (Leng and Kendziorski, 2019; Žiberna, 2018).

References

Chen, S., Zhou, Y., Chen, Y., Gu, J., 2018. fastp: an ultra-fast all-in-one fastq preprocessor. Bioinformatics 34, i884–i890.

Dobin, A., Davis, C.A., Schlesinger, F., Drenkow, J., Zaleski, C., Jha, S., Batut, P., Chaisson, M., Gingeras, T.R., 2013. Star: ultrafast universal rna-seq aligner. Bioinformatics 29, 15–21.

Gadagkar, S.R., Call, G.B., 2015. Computational tools for fitting the hill equation to dose–response curves. Journal of Pharmacological and Toxicological methods 71, 68–76.

Grier, H.E., Krailo, M.D., Tarbell, N.J., Link, M.P., Fryer, C.J., Pritchard, D.J., Gebhardt, M.C., Dickman, P.S., Perlman, E.J., Meyers, P.A., et al., 2003. Addition of ifosfamide and etoposide to standard chemotherapy for ewing's sarcoma and primitive neuroectodermal tumor of bone. New England Journal of Medicine 348, 694–701.

Hamid, R., Rotshteyn, Y., Rabadi, L., Parikh, R., Bullock, P., 2004. Comparison of alamar blue and mtt assays for high through-put screening. Toxicology in vitro 18, 703–710.

Harrow, J., Frankish, A., Gonzalez, J.M., Tapanari, E., Diekhans, M., Kokocinski, F., Aken, B.L., Barrell, D., Zadissa, A., Searle, S., et al., 2012. Gencode: the reference human genome annotation for the encode project. Genome research 22, 1760–1774.

Jang, I.S., Neto, E.C., Guinney, J., Friend, S.H., Margolin, A.A., 2014. Systematic assessment of analytical methods for drug sensitivity prediction from cancer cell line data, in: Biocomputing 2014. World Scientific, pp. 63–74.

Leng, N., Kendziorski, C., 2019. EBSeq: An R package for gene and isoform differential expression analysis of RNA-seq data. R package version 1.24.0.

Patro, R., Duggal, G., Love, M.I., Irizarry, R.A., Kingsford, C., 2017. Salmon provides fast and bias-aware quantification of transcript expression. Nature methods 14, 417.

Soneson, C., Love, M.I., Robinson, M.D., 2015. Differential analyses for rna-seq: transcript-level estimates improve gene-level inferences. F1000Research 4.

Žiberna, A., 2018. Generalized and Classical Blockmodeling of Valued Networks. R package version 0.3.4.